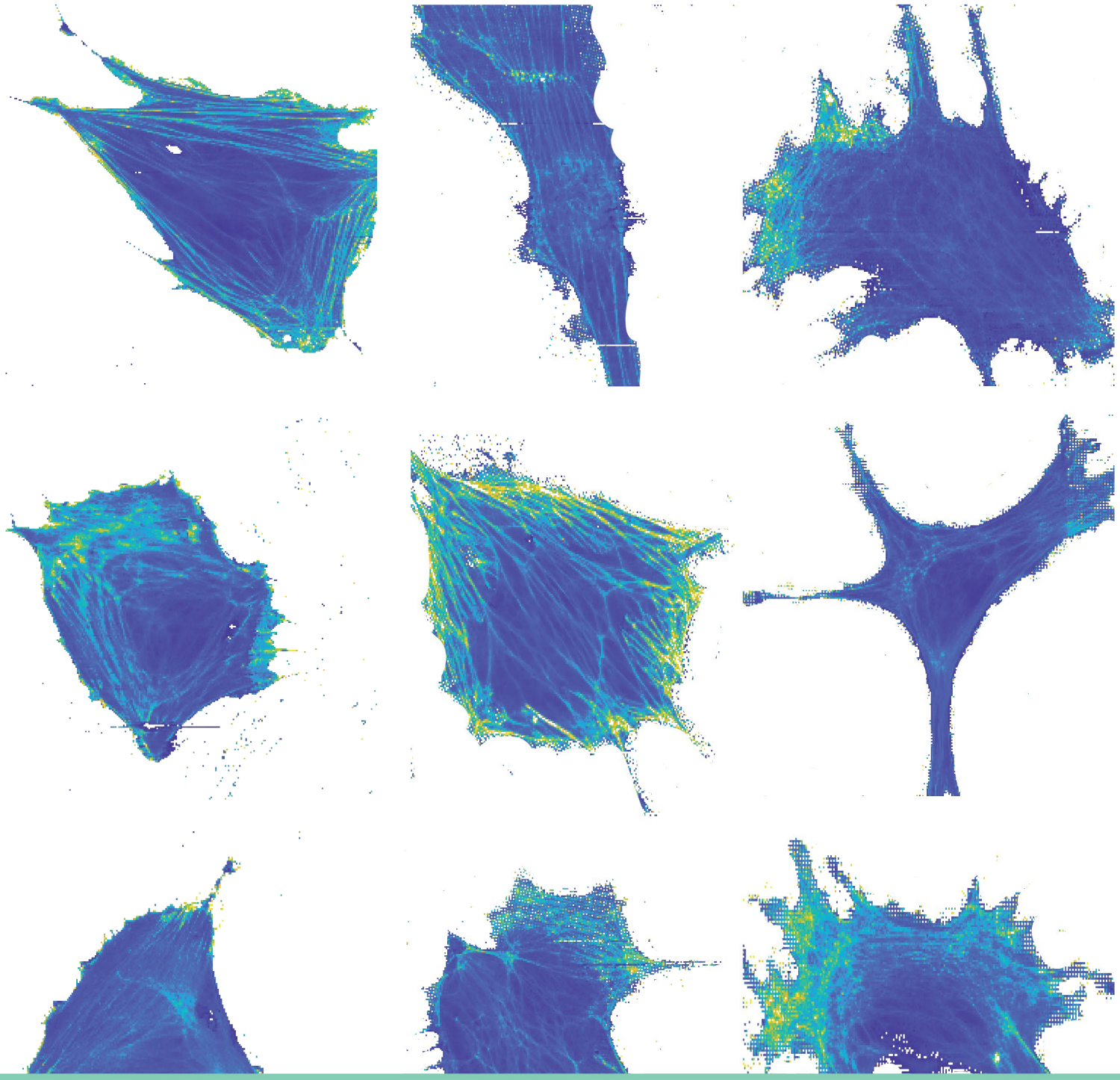

# Cell adhesion on 3D printed submicron patterns: a quantitative study

Bogdan Popa

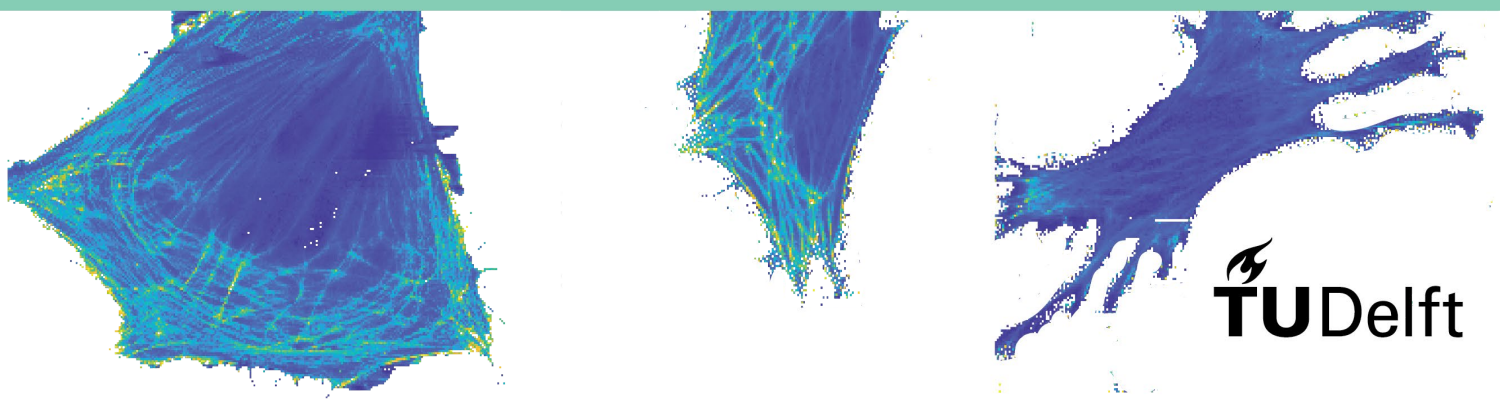

TU Delft

Page intentionally left blank

# Cell adhesion on 3D printed submicron patterns: a quantitative study

By

**Bogdan Popa**

In partial fulfilment of the requirements for the degree of

**Master of Science**
in Biomedical Engineering, Medical Devices and Bio-electronics Track

at the Faculty of Mechanical, Maritime and Materials Engineering of
**Delft University of Technology**

To be defended publicly on Wednesday, 16th of December, 2020, at 15:00

Thesis supervisors: Dr. ir. L.E. Fratila-Apachitei, TU Delft
Dr. ir. L. Angeloni, TU Delft
Dr. ir. M.K. Ghatkesar, TU Delft
M. Nouri-Goushki, TU Delft
Prof. Dr. A.A. Zadpoor, TU Delft

TU Delft

Student number: 4945034
An electronic version of the dissertation is available at:
repository.tudelft.nl/

Page intentionally left blank

# Preface

Before I start to dive deep into the scientific aspects of my work, I would like to express my gratitude to Lidy Fratila-Apachitei for the amazing opportunity offered and for all the guidance offered, week in, week out. I felt her support throughout the project, even when this support had to travel from her computer, thousands of kilometres into space and then back to my computer. And I would also like to thank Lidy for putting me in contact with a group of amazing people. Among these people, I must say a big thank you to Livia Angeloni for guiding me through the intricate and forever surprizing world of atomic force microscopy and for the immense amount of patience she had in all this process. My appreciation goes to Murali Ghatkesar as well, who has always come with a different perspective on my work, with each discussions pushing me a little bit further in understanding what I am doing but also why I am doing it.

I would also like to thank Mahdiyeh Nouri-Goushki for always being a pillar of stability in my endeavours into the universe of two photon polymerization. My work for this thesis started with her and it helped me lay the foundations for all the experiments that came after. And speaking of beginnings, I have to also thank Michelle Minneboo, who patiently and joyfully helped me start my work in the cell lab. Above all, I have to thank all of the people above for the empathy they showed, something that should never go un-noticed.

My project was also made possible by the help and assistance of Sander Leeflang, who helped me stay healthy and in one piece throughout the last year. Last but not least, I would like to thank Nazli Tumer as well for helping me comprehend my data and for pushing me in my understanding of statistical analysis.

Stepping outside the realm of the university, I would not be here without my family, Alina, Lucian and Andra (my only and also favourite sister), who above all thought me to be happy and make the most of every little thing around me. My everyday life would be very dull without my friends, who I have to thank for all the support, which came in all shapes and sizes, from Skype calls to sharing good food to taking me onboard on all sorts of photoshoots around the TU campus.

Page intentionally left blank

# Table of Contents

**Nomenclature**

| | |
|---|---|
| MSC | Mesenchymal stem cells |
| FFM | Fluid force microscopy |
| THA | Total hip arthroplasty |
| ECM | Extra-cellular matrix |
| AFM | Atomic force microscopy |
| SCFS | Single cell force spectroscopy |
| CAD | Computer aided design |
| 2PP | 2 photon polymerization |
| PEG | Polyethylene glycol |
| QI | Quantitative imaging |
| SEM | Scanning electron microscope |
| α-MEM | α minimum essential medium |

## Abstract

**Objectives:** With an increasing life expectancy in the western societies and more people practising extreme sports, the demand for orthopaedic implants is set to increase. Orthopaedic implant loosening is one of the main causes of revision surgeries, leading to increases in the costs of patient care and patient dissatisfaction. Better osseointegration could lead to higher success rates of primary interventions. Mesenchymal stem cells (MSC) can undergo osteogenic differentiation on the implant surfaces, promoting the implant osseointegration. Alternatively, they can commit to other differentiation paths (*e.g.,* fibroblasts) and thus hinder the osseointegration and functionality of the implant. It is therefore fundamental to promote the osteogenic differentiation of MSC at the surface of the implant to ensure enhanced osseointegration and thus its long term success. Among the available strategies that promote osteogenic differentiation, nano and micro-scale physical patterns have proved effective but the underlying mechanisms that induce these cellular changes are not yet understood.

Cellular adhesion to the surface is believed to be the key process regulating mechanotransduction (*i.e.,* extrinsic cell signalling) and subsequently, the mesenchymal stem cell osteogenic differentiation. Nevertheless, no quantitative systematic study has been performed in order to establish the relationship between the cell adhesion and the differentiation behaviour. Furthermore, the available cellular adhesion studies are only qualitative or semi-quantitative in nature. In this work, novel fluid force microscopy (FFM) technique has been employed to characterize the adhesion properties induced by a set of osteogenic and a set of non-osteogenic submicron patterns.

**Methods:** Two sets of substrates consisting of arrays of submicron pillars with known osteogenic potential were manufactured by means of two photon polymerization. Preosteoblast mouse cells were cultured on the patterns and on a flat control surface. The adhesion properties (*i.e.,* the force and work of adhesion) were measured by FFM after 4 and 24 hours of cell culture. The cellular behaviour picture was completed by assessing the Young's modulus of the living cells attached on the patterns and on the control surface. Likewise, the topographical and mechanical mapping was performed by using atomic force microscopy system.

**Results:** In this study, the adhesion of preosteoblast cells was successfully quantified on two types of submicron pattern with known osteogenic potential, and compared to cellular adhesion data on a flat control. Therefore, the fluid force microscopy (FFM) was applied for the first time. The trend indicated that cells seeded on the osteogenic substrate adhered stronger (mean force of adhesion = 159 ± 74 nN) than cells on the non-osteogenic substrate (mean force of adhesion = 108 ± 104 nN) after 24h of incubation. Moreover, the cells adopted different morphologies and spatial distribution of the Young's modulus depending on the culture substrate.

# 1. Introduction

The number of implants used in medical care has seen a substantial increase in the last half century. Among the most commonly employed types of implants are the orthopaedic implants. Western societies face an aging population, people who develop diseases such as arthritis, and an increasing number of people engaging in extreme sports that can lead to injuries. The increasing demand for these implants also leads to an increase in healthcare costs associated with these interventions [1,2]. In the Netherlands alone there were 31,154 primary total hip arthroplasties (THA) in 2018 [3]. Additionally, there were 3,788 revision THAs (*i.e.,* patients undergoing a second operation related to their implant), 40,4% of which were caused by components loosening [3]. Better integrated implants with the host bones may lead to a decrease in post-operative complications and costs associated with these interventions and also an increase in patients satisfaction.

Mesenchymal stem cells (MSCs) are among the first reparative cells to arrive at the site of implantation and start to interact with the environment. They can undergo osteogenic differentiation promoting the osseointegration, or they can differentiate into other kinds of cells (*e.g.,* fibroblasts), significantly affecting the osseointegration and the functionality of the implant [4]. Therefore, understanding the cell – surface interactions is crucial for developing effective bone implants [5]. In addition to the intrinsic cellular gene activation pathways that lead to proliferation, migration or differentiation, the cells also receives extrinsic signals, from the extracellular matrix (ECM) that can guide the cellular evolution. The complex nature of the hierarchical organization of the bone provides cues to cells at all levels, from the macroscale to the nanoscale. Traditionally bone implants have focused on recreating the macroscopic environment of the bone [6].

The biomaterials study field is evolving and shifting towards biologically active devices that can improve the implant's functionality. One of the research paths chosen to develop these novel solutions are materials that propose the instruction the cellular behaviour [2]. The instruction strategies can be classed in three categories: chemical cues [7], mechanical [8] or physical [4]. Recent work [9–13] has highlighted the power of submicron patterns on MSCs or pre-osteoblast cells. The right pattern design leads to the expression of proteins specific for osteogenic differentiation [9,10] and matrix mineralization [9]. The research of physical cues is also pushed by the novel manufacturing technologies that have developed to allow precise micro and nano manufacturing [14,15].

Nevertheless, in order to understand the effects of these submicron patterns on stem/progenitor cells fate, the literature focuses mainly on whether a substrate can or cannot induce the osteogenic differentiation and/or matrix mineralization. These tests usually assess the final state of cells, after at least 21 days of incubation and thus, potential important information on early cellular morphological and adhesive properties is missing. These properties can play an important role in further differentiation and ECM formation. A better understanding of the adhesion behavior of cells on the surfaces would enable the elucidation of the cause-effect relations with regard to surface-induced effects, and provide extra tools to enhance the osteogenic potential of biomaterials. In addition, such studies can lead to establishment of novel biomarkers that could be used to more rapidly screen the osteogenic potential of biomaterials.

A wide variety of qualitative/semi-quantitative methods is employed in the literature to study cellular adhesion. They can describe the amount and area of focal adhesion sites (by fluorescence microscopy [16]), approximate detachment stress for a population of cells (by fluid flow chamber

assays [17]) or the expression of adhesion related proteins (by colorimetric assays [18]). Nevertheless, novel atomic force microscopy (AFM) based techniques can be used to quantitatively determine the adhesion properties of single cells [19,20]. Single cell force spectroscopy [19] (SCFS) is employed to study the very early adhesion (up to 2 minutes) by chemically attaching the cell to the AFM probe. This bonding already activates adhesion related signalling pathways [21] before the cell even touches the substrate of interest. FFM is a novel approach to the problem that proposes mechanically gripping the cells by means of vacuum through a micro-channel integrating AFM probe [20]. Moreover this approach allows for longer incubation times before the detachment of cells (*e.g.,* three days [22]). No quantitative information is currently available on the adhesion of cells on surfaces with specific topographies and thus it makes FFM an attractive technique to be employed in the quantification of cellular adhesion on these topographies.

As already mentioned, submicron patterns consisting of pillars with specific sizes and spatial organization have recently shown potential to induce osteogenic differentiation of preosteoblasts [10]. In this project, the FFM method was used for the first time to quantitively study the adhesion behavior of preosteoblasts on these patterned surfaces. In order to conduct this investigation, several objectives were set:

- Fabrication and characterization of submicron patterns: two different patterns were included in the study next to a flat control.
- Assessment of morphological and mechanical properties of living cells seeded on the three substrates for two different incubation times
- Quantification of cellular adhesion properties after the two incubation times

# 2. Materials and methods

## 2.1. Pattern design and fabrication

The submicron patterns have been designed based on the previous work of Nouri-Goushki *et* al [10]. They included arrays of pillars with a diameter of 200 nm, an interspace of 700 nm and two different heights, 500 nm and 1000 nm (Figure 1a). The pattern with pillars having 500 nm height was non-osteogenic (denoted N-OST in this report) while the patterns with pillars having 1000 nm height was osteogenic (denoted OST in this report). The individual pillars were designed with the help of a computer aided designed (CAD) software (Solidworks, Dassault Systèmes SE, France). The CAD files were converted to STL files and further processed in the DeScribe software (NanoScribe GmbH, Germany) (Figure 1b,c). The single pillar STL file was the starting point to create a 40x40 µm array of pillars. The array was then multiplied to form a 1x1 $mm^2$ pattern. The DeScribe code used to generate the submicron patterns is available in Appendix A.

The printing was performed by a Photonic Professional GT+ system, a two photon polymerization (2PP) solution offered by NanoScribe GmbH (Germany). The system worked on the basis of a pulsed femtosecond laser (centre wavelength = 780 nm, pulse duration = 100 fs, repetition rate = 80 MHz, maximum laser power 50 mW). The laser beam was focused through a 63x objective (numerical aperture = 1.4). Printing was conducted in the immersion lithography mode (conventional mode) (Figure 2a), *i.e*., in the positive z direction, using the conditions presented in Figure 2b. The glass slide was cleaned with acetone (Sigma-Aldrich, Germany) and rinsed with isopropyl alcohol (IPA, Sigma-Aldrich, Germany) before being loaded in the 2PP system.

a)

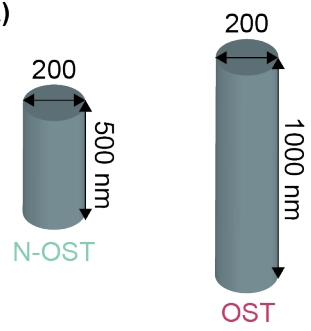


b)

| Parameter | Value (µm) |
|---|---|
| Hatch distance (1) | 0.05 |
| Slice distance (2) | 0.15 |
| Horizontal interspace | 0.7 |
| Vertical interspace | 0.7 |

c)

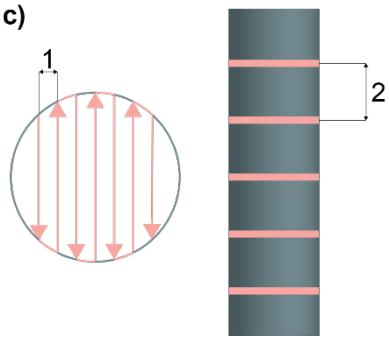


**Figure 1.** (a) Render image of the two types of pillars employed in the study; (b) table describing the STL file processing parameters; (c) figure depicting the hatching distance and laser scanning directions (1) and slicing distance (2)

The oil used for objective immersion and the photo-sensitive resin were Immersoil and IP-L780, provided by NanoScribe GmbH (Germany). After the printing job was finished, the sample went through a two-step development process, with the aim of removing the oil and non-polymerized resin from the glass substrate. During the first step the sample was submerged in propylene glycol methyl ether acetate (Millipore Sigma, Germany) for 25 minutes. For the second step the sample was submerged in isopropyl alcohol for 5 minutes. For cell experiments, the glass slides containing the submicron patterns were glued onto a petri dish (TPP, Switzerland), using a two part structural body epoxy, EA 9492 (Loctite, Germany).One additional type of structure was printed using the same set-up and printing conditions: a solid block of polymer (30 x 30 x 10) µm for assessing the bulk material's Young's modulus.

a)

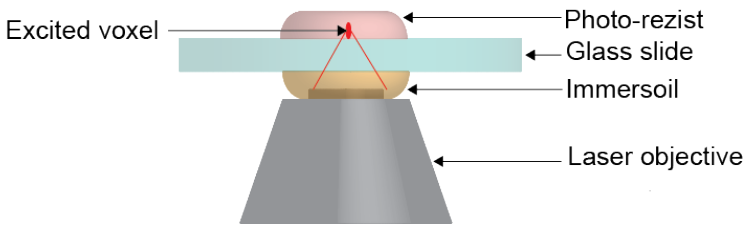


b)

| *Parameter* | *Value* |
|---|---|
| Laser power | 14% |
| Scan speed | 1200 µm/s |
| Interface position | -200 nm |

**Figure 2.** (a) Schematic representation of printing set-up; (b) table presenting printing parameters, where the laser power is a percentage of the maximum laser power and interface position represents the depth into the substrate where the laser scans the first layer.

## 2.2. Pattern characterization

### 2.2.1. Bulk material mechanical characterization

Elastic modulus of the pillars material was tested using an AFM system, JPK NanoWizerd 4 (Bruker Corporation, USA) with a NM-TC probe (Bruker Corporation, USA). Both the tip and the cantilever of the probe were fabricated out of diamond, and thus enabling accurate indentation of the block of polymer, without damaging the probe. The cantilever had a nominal length of 125 µm, width of 30 µm and a spring constant of 350 N/m. The thermal calibration method [23] was not feasible in this case due to the high stiffness of the cantilever and thus the relative method of calibration was used [24].

Firstly, a substrate of similar elastic modulus to the cantilever (sapphire was used in this case) was indented with a setpoint of 0.4 V, in contact mode. The resulting force-distance curve was then used to compute the probe sensitivity by fitting the approach slope of the force-distance curve (sensitivity

= 29.27 nm/V). Secondly, the indented surface was changed to a material of known elastic modulus, the back side of a petri dish (TPP, Switzerland) (polystyrene, elastic modulus of around 3 GPa). The polyethylene glycol (PEG) surface was scanned in quantitative imaging (QI) mode with a set surface indentation of 56 nm (set point was set at 10 nm, z length at 1000 nm and pixel time at 8.3 ms). The data was then fit using a Hertz-Sneddon curve fit model, by setting the tip shape to “paraboloid” and iteratively changing the tip radius until the resulting recorded elastic modulus was approximately 3 GPa (tip radius = 6 nm). The same scan parameters and probe properties were kept constant throughout the scans performed on the solid block of polymerized resin. Nominal spring constant was used for these measurements. The acquired image resulted in 65,536 points (a 256x256 pixels image) containing the local elastic modulus value. The elastic modulus of the polymerized material is reported here as the mean and standard deviation of the recorded values.

### 2.2.2. Pattern morphological characterization

#### Atomic force microscopy imaging

Submicron patterns topographical characterization was performed using AFM. The system used was the JPK NanoWizard 4 (Bruker Corporation, USA), with a TESPA-HAR probe (Bruker Corporation, USA). The cantilever had a width of 40 µm, a length of 125 µm and a nominal spring constant of 42 N/m. The tip had a nominal radius of 10 nm and a high aspect ratio (length of approximately 2 µm). It was manufactured out of antimony doped Si. Probe calibration was conducted using the thermal method [23]. The probe had a high aspect ratio tip that can scan both the pillars and the underlying glass slide accurately (Figure 3).

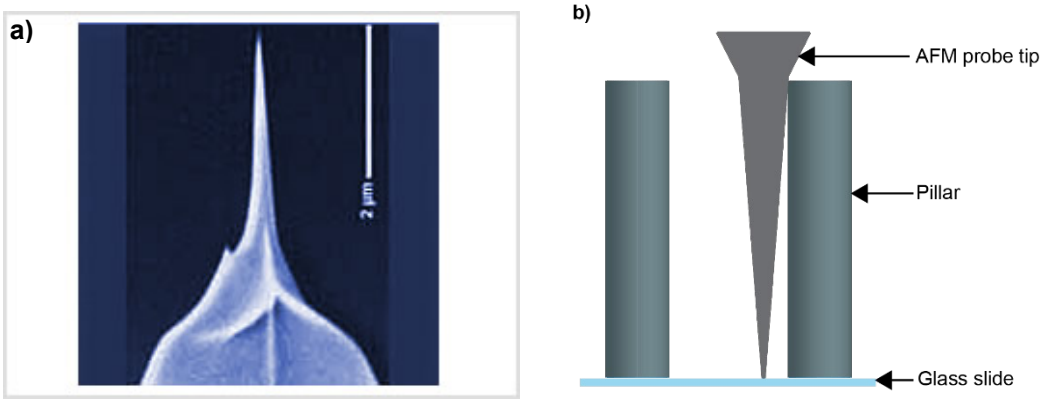


**Figure 3.** (a) SEM image of AFM probe tip used for submicron pattern topographical characterization (image reproduced from the Bruker Corporation website); (b) probe tip positioning while scanning the submicron pattern (not to scale)

The topographical images of the pillars were acquired in QI mode, with the following scanning parameters: setpoint 100 nN; z length 1500 nm; pixel time 16 ms. A 10 x 10 µm area was scanned on three N-OST and OST submicron patterns and a height profile going over the tips of 13 pillars was selected to evaluate the pillars height and the pillars interspace. In total 39 data points/pattern were analysed for both height and interspace.

The morphological image was exported as a text file (in the shape of a 256 x 256 matrix containing the height values) from the JPK Data Processing software (Bruker Corporation, USA). The image was then reconstructed in MATLAB (MathWorks, USA) as a colour map. The submicron height map generation code is available in Appendix B. The roughness of the patterns was assessed in the JPK Data Processing software.

### Scanning electron microscopy imaging

The diameter of pillars was assessed with the help of scanning electron microscopy (SEM) images. The system used was Helios Nanolab 650 (FEI, USA). Samples were gold sputtered, up to a thickness of ≈ 5 nm, using a JFC-1300 (JEOL, Japan) sputter coater and then imaged with the SEM system, at 30° inclination. The images were analysed with the ImageJ software (rsb.info.nih.gov/ij/index.html). Inter-used variability is present in the data as the measuring points were set manually. The diameter of 39 pillars from three different regions of one sample was measured at midpoint between the base of the pillar and the tip of the pillar.

## 2.3. Cell culture

The cells used in this study were mouse pre-osteoblast, MC3T3-ε1 (Sigma-Aldrich, Germany). 5 x $10^4$ (passage 11) were pre-cultured in a 6-well plate (Greiner Bio-One, Netherlands) in alpha minimum essential medium (α-MEM) (ThermoFisher, USA), supplemented with 10% fetal bovine serum (FBS, ThermoFisher, USA) and 1% penicillin-streptomycin (ThermoFisher, USA). Cells were incubated (at 37°C and 5% $CO_2$) for at least 3 days (medium changed every two days) before seeding them on the substrates of interest for the experiments. Cells were detached from the 6-well plate by incubating them in 100 µl trypsin (Sigma-Aldrich, Germany) for 5 minutes.

**Table 1.** Overview of experimental conditions and the measured outcomes

| *Substrate* | *Time points* | *Investigate* |
|---|---|---|
| Control (borosilicate glass) | 4h | Force of adhesion |
| N-OST submicron pattern | 24h | Work of detachment |
| OST submicron pattern | | Cell morphology |
| | | Cell Young's modulus |

The substrates were sterilized by immersion in 70% ethanol (Sigma-Aldrich, Germany) before usage. The density of seeded cells had to be large enough to ensure that enough cells adhere to the 1x1 mm area of the submicron pattern, without the cells forming intra-cellular connections. Therefore, 7,5 x $10^4$ cells were seeded on a substrate for experiments starting after 4h of incubation and 5 x $10^4$ cells were seeded on a substrate for experiments starting after 24h of incubation. The protocols used for cell culture are presented in detail in Appendix C.

## 2.4. Cell morphological and mechanical characterization

Cells adherent on the three surfaces were scanned using the QI mode, with a qp-BioAC-CI-10 CB3 probe (cantilever had a length of 80 µm; width of 30 µm, tip radius of 30 nm and a nominal spring constant of 0.06 N/m) (Nanosensors, Switzerland) with an AFM system (JPK NanoWizerd 4, Bruker Corporation, USA). The QI scanning resulted in a mechanical map and a topographical image corresponding for the same scanned area. The probe (manufactured out of quartz-like material) was calibrated using the thermal method [23]. The sample (containing the culturing substrate, cells and 2 ml of α-MEM) was placed in a petri dish heater and maintained at 37°C. Single cells were scanned with a setpoint of 1 nN, z length of 2500 nm and a pixel time of 21 ms. The set point was equivalent to indentation depths in the range of 200 to 1000 nm. The image resolution was set to 256 x 256 pixels, over an area of 95 x 95 µm. Maps containing areas which were too tall for the probe to scan (resulting in a shadow or missing pixels) were discarded. Topographical maps were used to extract the height data about the cells. A line passing through the middle of the nucleus, across the

narrowest section of the cell, was analysed in the JPK Data Processing software (Bruker Corporation, USA). Cells shapes were classed as polygonal, stellate or polarized. 12 cells were scanned for each condition.

The mechanical maps were fitted using the Hertz-Sneddon model, with a paraboloid tip shape type. The mechanical and topographical maps were then exported to MATLAB (MathWorks, USA) as text files, containing the height and Young's modulus values. The Young's modulus values were filtered after the application of a low and high threshold (2 kPa and 80 kPa respectively) in order to remove the data points representing the substrates. The data was then reconstructed as colour maps. Young's modulus values were collected from all the cells in a certain condition and summarized in a box plot format. The MATLAB codes used for processing the data obtained from the QI scanning of cells are available in Appendix D and E.

A section corresponding to the nucleus of each mechanical map was selected in order to record the average Young's modulus value of the nucleus. As the section was manually chosen, it introduces inter-user variability. The data did not follow a normal distribution and the distributions did not follow the same shape. As a result, a Kruskal-Wallis statistical test was performed to test for statistically significant differences between the substrates. Moreover, Mann-Whitney tests was performed to test for differences between the 4h and 24h of incubation time points. A Bonferroni correction was applied in order to account for multiple tests (p value was deemed significant when it dropped under 0.016). The tests were performed with the SPSS software (IBM, USA).

A second batch of morphological data (cell area and shape) was acquired with an inverted optical microscope (Zeiss Axio Observer, Carl Zeiss AG, Germany). The cells were imaged before the detachment experiment and the measurements were conducted with the help of the ImageJ software (rsb.info.nih.gov/ij/index.html). Cell boundaries were set manually, thus introducing inter-user variability. 12 cells were imaged for the flat control and the OST (both at 4h and 24h) and N-OST (4h) conditions and 8 cells were imaged for the N-OST, 24h condition. The area data points obtained with the optical microscope were then included as a dependant variable in the statistical analysis of force of adhesion and work of adhesion (see section 2.5.), as all the data points come from the same individuals. Statistical analysis that compares the area between the different substrates is presented in section 2.5.

## 2.5. Cell adhesion properties

FFM measurements were based on the JPK NanoWizerd 4 (Bruker Corporation, USA). The FFM set-up was composed of parts sourced independently. The microfluidic probes (FluidFM micropipette) were acquired from Cytosurge (Switzerland). The cantilever had a length of 200 µm, width of 36 µm and a 2 N/m nominal spring constant. The probe was calibrated using the thermal method [23]. FluidFM micropipettes were manufactured out of silicon nitride. The aperture of the microfluidic channel, positioned at the end of the cantilever, had 8 µm in diameter (Figure 4a). The probe was filled with two times filtered de-ionised water before the start of experiments to ensure a liquid – liquid interface at the aperture. The tubing of the microfluidic system was assembled in-house using the available standard tubes and connectors. The pressure was controlled by OB1 fluid controller (Elveflow, France). A schematic of the system is presented in Figure 4b. AFM was used in contact mode (force spectroscopy option), with a CellHesion integrated system module (Bruker Corporation, USA) that extended the piezoelectric range in the vertical direction to 100 µm.

The sample (cells cultured on the substrate in α-MEM) was loaded in a petri dish heater that maintained a constant temperature of 37°C. Cell detachment process parameters were established by consulting literature articles [22,25] and Cytosurge's recommendations [26]. The aperture was always positioned over the cell nucleus which it approached with a speed of 1 µm/s until it indented the cell with a force of 50 nN. The cell indentation was followed by a 10 s pause, during which the probe kept a constant force over the cell and the pressure controller is turned on to create vacuum and thus a suction force (Figure 4c). The under-pressure (vacuum) was adjusted according to the requirements of the cells: large cells required a stronger vacuum (-800 mbar) while -500 mbar was enough to grip small cells throughout the retract movement of the cantilever. The need for vacuum pressure adjustment according to the size of the cells was also reported by Sztilkovics *et al* [27]. Once the pause was over, the probe started to retract (move upwards) with a speed of 1 µm/s. The range of vertical movement was set to 80 µm and the under-pressure was maintained throughout the retraction stage of the movement.

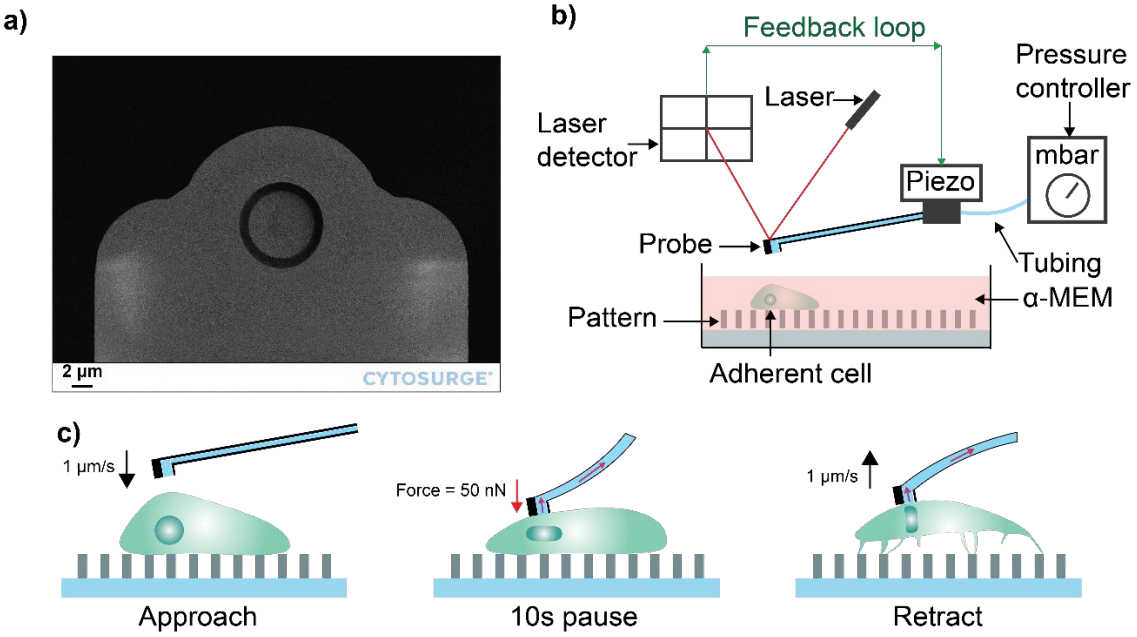


**Figure 4.** (a) Tip SEM image of one of the micro-fluidic probes used during the experiments (image reproduced from the Cytosurge database); (b) Schematic of the FFM set-up, integrated with the AFM system; (c) schematic sequence showing the steps of cell detachment during an FFM experiment: probe approaches the cell, probe indents the cell up to the set force and the vacuum is applied in order to mechanically grip the cell to the probe, probe starts the retract movement and thus breaks the adhesion between the cell and substrate

After each interaction with cells, the probe was submerged in Terg-a-zyme (Alconox Inc., USA) 1% solution for 2 minutes for cleaning, followed by rinsing in double filtered de-ionised water [26]. On average a probe was used to detach 4 cells before the microchannel clogged with cellular debris (Appendix F). 12 cells were detached for each condition and for each cell the force of adhesion ($F_{adh}$) and work of adhesion ($W_{adh}$) is reported. Data collected from failed detachments (partial detachment of cells, broken cellular membrane during the retraction of the cantilever or detachment by means of suction) were discarded. The FFM protocol presented in detail in Appendix G.

The JPK Data Processing Software was used for the processing of the FFM FD curves. A noise filter was used to reduce the recorded noise, before the axis were set: Y-axis was set to be in line with the baseline of the retraction part of the FD curve while the X-axis was set to 0 at the point the approach curve reveals the cell-probe contact point. The software calculated then the force of

adhesion and the work of adhesion. The FD curves data was then exported as a text file to MATLAB (Appendix H) for plotting.

The statistical analysis was conducted using SPSS software (IBM, USA). Data was not normally distributed and the distribution of data for different conditions did not follow the same shape. The test chosen in this case was a Kruskal-Wallis test (also known as a non-parametric one-way ANOVA). Data points were ranked and the mean rank of each condition was compared. As the data did not follow the same distribution shape, SPSS compared the mean ranks of each condition. A Bonferroni correction was applied to take multiple tests into account. The threshold for statistical significance was set at $p = 0.05$. Correlation between dependent variables was tested with the Pearson rho test. The threshold for statistically significance correlations was set at $p = 0.01$. In the figures a value of $p < 0.05$ is marked with "*" and $p < 0.0001$ with "****".

# 3. Results

## 3.1. Pattern morphological features and mechanical characterization

For both patterns, the pillars' interspace and diameter were consistently reproduced both within the 1 x 1 $mm^2$ printed area of a sample as well as between different samples (Table 2, Figure 5). Height deviations were more present for the N-OST pillars (Table 2). The relatively larger variability in the height of N-OST pillars can be attributed to the voxel shape and size: the ellipsoid voxel had a height in the range of 500 to 1000 nm (empirically established) [28]. With a voxel (a volume in which the photoresist is prone to polymerization) taller than the structure to be printed, it can be expected that undesired polymerization occurs around the exposed pillar. This aspect is mitigated by the choice of a low laser power (14%, see Figure 2b). Moreover, the voxel shape [28] leads to a decrease in diameter towards the tips of the pillars, *i.e.,* pillars became ellipsoidal at the tip (Figure 5, see Appendix I). SEM images of the patterns are presented in Appendix I. The roughness increased with the increase in height. The printing times of the 1 x 1 $mm^2$ submicron patterns were 10h30min for the N-OST and 15h40min for the OST. Polymerized bulk material returned an elastic modulus of 3.8 ± 0.2 GPa.

**Table 2.** Measured feature dimensions of pillars (mean ± SD)

| *Pattern* | *Height (nm)* | *Interspace (nm)* | *Diameter (nm)* | *Ra (nm)* |
|---|---|---|---|---|
| N-OST | 460.8 ± 63.3 | 701.8 ± 17.3 | 204.6 ± 10 | 113.5 ± 1 |
| OST | 1034 ± 30.5 | 692.6 ± 24.2 | 199.3 ± 9.6 | 235.6 ± 8.5 |

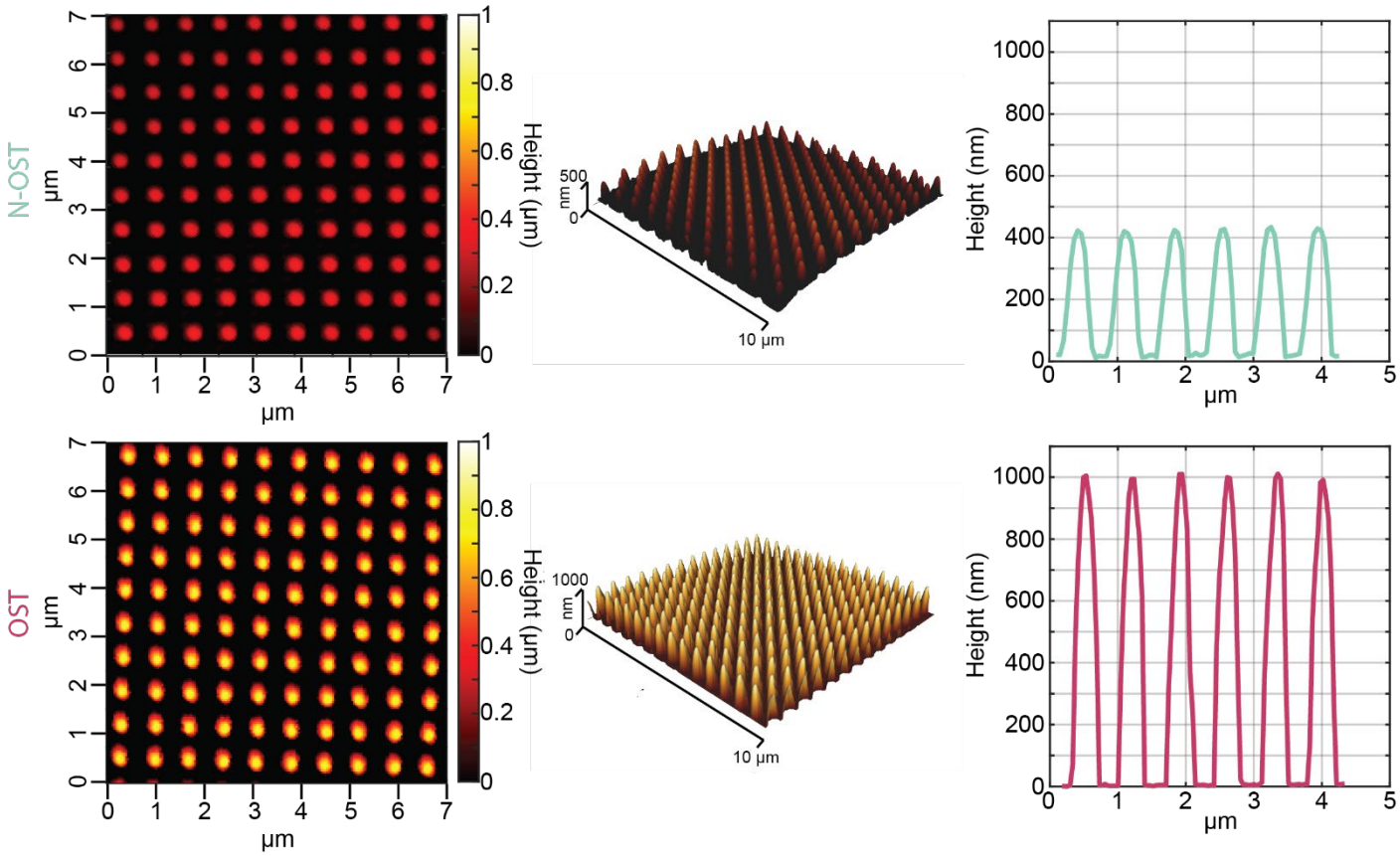


**Figure 5.** (Top row) results of AFM measurements of the N-OST submicron pattern; (bottom row) results of AFM measurements of the OST submicron pattern: height map (left column), 3D reconstruction of the height map (middle column), profile following a line through the centres of the pillars (right column)

## 3.2. Cell morphology

Representative morphologies of the living cells can be observed in Figure 6, for all the conditions investigated. The flat control substrate facilitated spreading of the cells and this can be seen in the area comparison (Figure 7a). Cells cultured on flat control had the highest area (mean area of 2637 ± 708 µm$^2$ at 4 h and of 5860 ± 3083 µm$^2$ at 24 h). The variability in cell area was the highest in the case of flat control, while cells seeded on the OST submicron pattern presented the smallest degree of variability (Figure 7a). Cells cultured on the OST submicron pattern had the lowest level of cell spread, *i.e.*, the measured area was the smallest out of the tested conditions (mean of 1287 ± 589 µm$^2$ at 4h and 1282 ± 733 µm$^2$ at 24h). The area in this condition was significantly different from the area in the control condition ($p < 0.0001$ at 4h and 24h) (Figure 7a). Area of cells seeded on the N-OST showed intermediate values (1798 ± 612 µm$^2$ at 4 h and 1962 ± 800 µm$^2$ at 24 h), being significantly different from the area of cells on flat control at 24 h ($p < 0.05$). Area of cells cultured on submicron patterns stayed constant between the 4 h and 24 h time points, while the area of cells on the flat control doubled on average. The height of cells measured in the nucleus area was relatively equal on all substrates, independent of the time of incubation (Figure 7b).

In addition, different cell shapes were observed on the different surfaces. Cells seeded on the flat control evolved predominantly into polygonal cells (62.5% at 4h and 75% at 24h). Stellate cells were only present in proportion of 29.2% at 4h and 8.3% at 24h while polarized cells represented 8.3% at 4h and 16.7% at 24h of the total number of cells cultured on the flat control (Figure 7c). Cells cultured

on the N-OST developed into a relatively equal share of all three types of shapes both at 4h (20% polygonal, 33% stellate, 45% polarized) and 24h (25% polygonal, 20% stellate, 55% polarized). Almost none of the cells cultured on the OST submicron pattern revealed a polygonal shape (0% at 4h and 4.2% at 24h), instead presenting a relatively equal evolution into stellate and polarized cells both at 4h (50% stellate, 50% polarized) and 24h (54% stellate, 41% polarized) (Figure 7c).

In summary, the patterns induced differences in cell area and cell shapes relative to the flat control. The trend indicated smaller cells, and more polarized and stellate cells on the patterns relative to the flat control. Between the two patterns, the only difference was noticed with regard to the shape of the cells, the OST pattern (with the taller pillars) inducing the highest proportion of stellate cells with long and thin filopodia clearly visible after 24 h of culture.

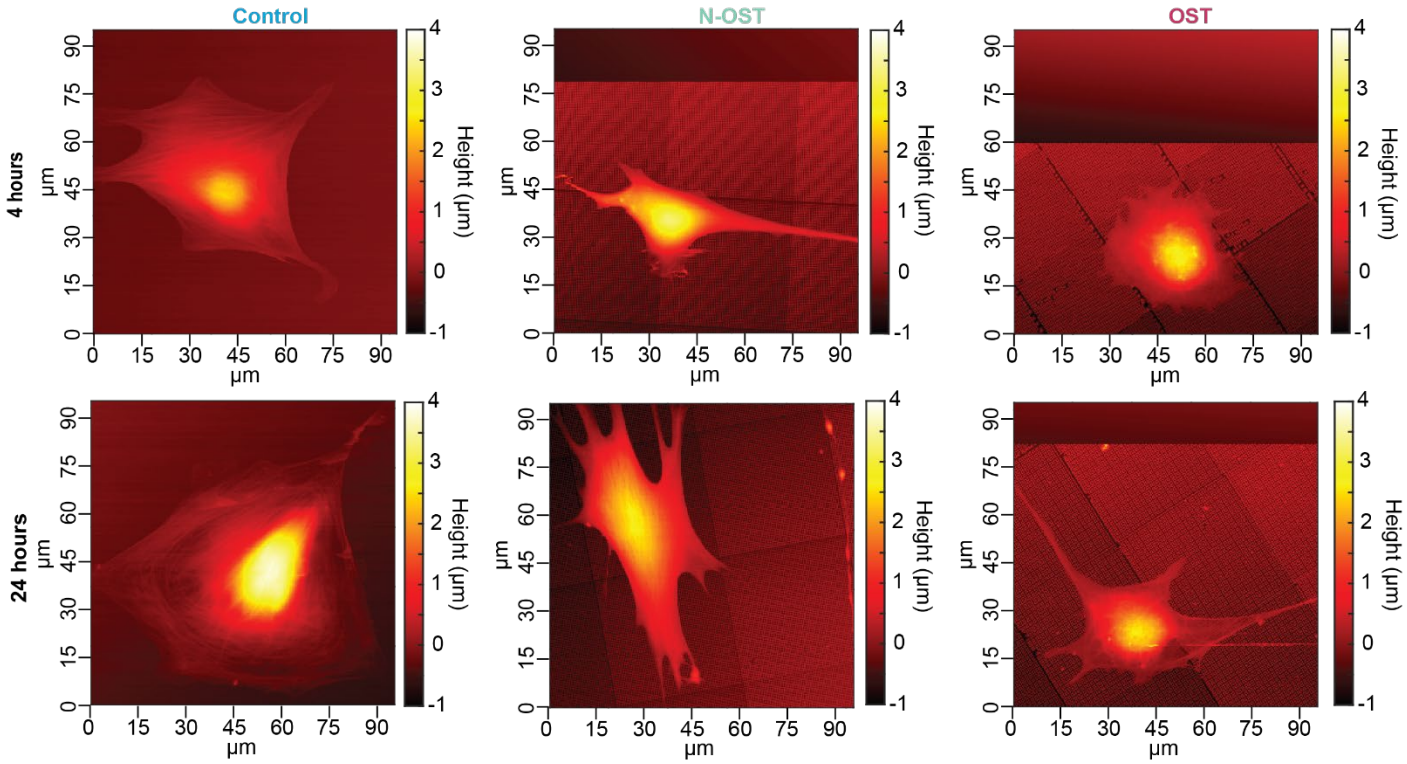


**Figure 6.** Height maps of live cells. The underlying pillars can be observed for cells cultured on the submicron patterns (middle and right columns). In these examples, cells in the control conditions are examples of polygonal cells, cells in the N-OST condition are examples of polarized cells and the cell exemplified for the OST condition counts as a stellate cell.

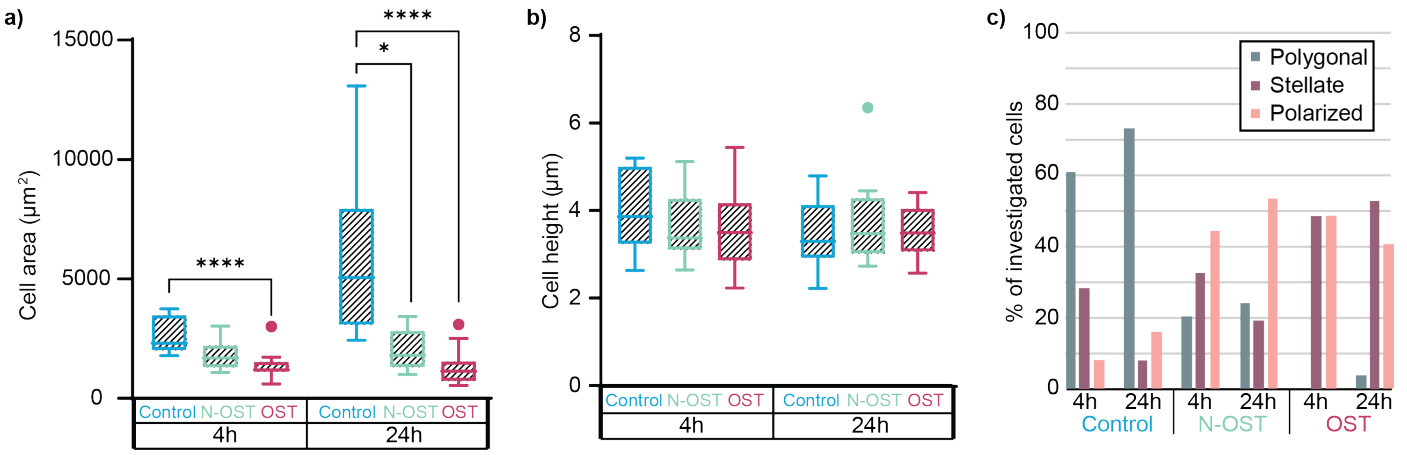


**Figure 7.** Summary of morphological measurements of cells, after 4h and 24h of incubation on the three types of substrates: (a) area, (b) cell height (nucleus area). The box plots were plotted using the Tuckey's method. (c) Cell shapes on the different substrates. Non-parametric one-way ANOVA (Kruskal-Wallis test) was used to test for statistically significant differences (* $p < 0.05$; **** $p < 0.0001$)

## 3.3. Mechanical characterization of living cells

The mechanical maps (Figure 8) reveal the Young's modulus of cells. For data analysis, the threshold applied to the Young's modulus values acted less effectively on the submicron patterns as the structures induced a higher amount of noise than the flat control (Figure 8). The Young's modulus of cells in the nuclear region was relatively equal across all substrates, in the range of 5 to 10 kPa with no significant differences between the 4 and 24 h of incubation time points, except for the N-OST pattern (Figure 9a). The average Young's modulus of single cells recorded after 4h of incubation were between 14 kPa for cells attached on the flat surface and 20 kPa for cells attached on the OST pattern (Figure 9b). After 24 h of culture the average Young's modulus of cells varied between 18 kPa on the control to 22 kPa on the OST pattern, with no significant differences between the different surfaces. The differences in overall Young's modulus go against the observations based on Young's modulus mechanical maps. This aspect can be linked to the higher amount of noise present in the submicron patterns, which artificially increases the average values of the scanned areas.

The fibres pattern observed on the cells seeded on the flat surface after 4 h of culture (Figure 8) can be associated with the actin stress fibres developed by these cells. After 24h of incubation, fibrous structures were still present in the cells seeded on the flat control while cells cultured on the N-OST substrate developed these fibres as well. By comparison, cells cultured on the OST substrate did not show such clear fibres in the cell body (Figure 8).

The arrangement of fibres within the cells differed according to cell shapes as well (Figure 8). Polygonal cells developed fibres with no dominant orientation, organized around the nuclei. In polarized cells, the fibres aligned along the direction of elongation, creating a dense fibre structure crossing in many cases over the nuclei. In the case of stellate cells, higher Young's modulus values were associated with the filopodia, while the cell bodies appeared 'mechanically' more homogeneous.

In summary, no significant differences in the Young's modulus of cells attached on the three different surfaces were found after 4 and 24 h of culture. In addition, the Young's modulus maps revealed a

heterogeneous distribution associated with a different cytoskeleton organization of the cells attached on the different surfaces.

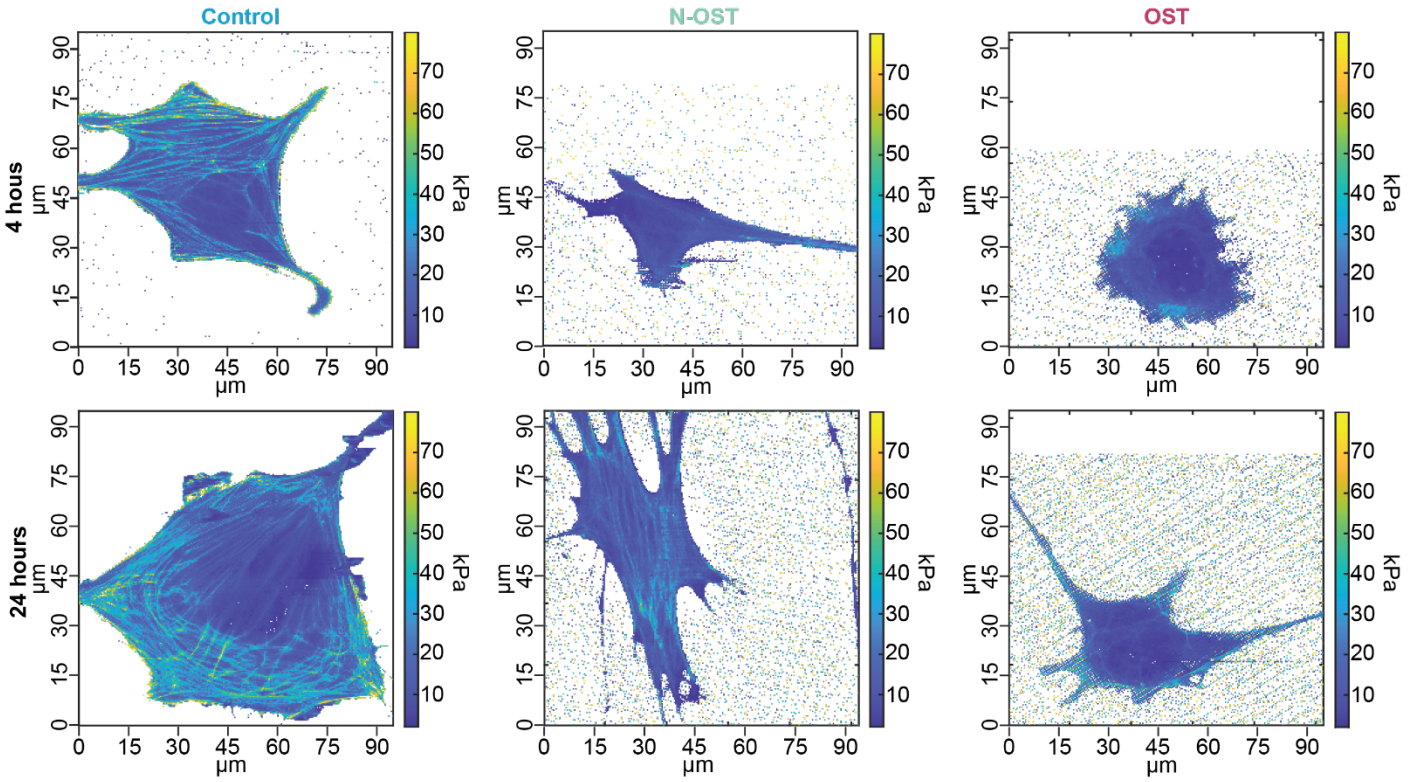


**Figure 8.** Young's modulus (kPa) maps of representative cells for each condition. Fibre structures were prominent for cells seeded on the flat control after 4h of incubation already. Cells seeded on flat control and N-OST generally revealed well defined fibre structures while the cells cultured on the OST submicron pattern appeared more homogeneous both after 4h and 24h of incubation.

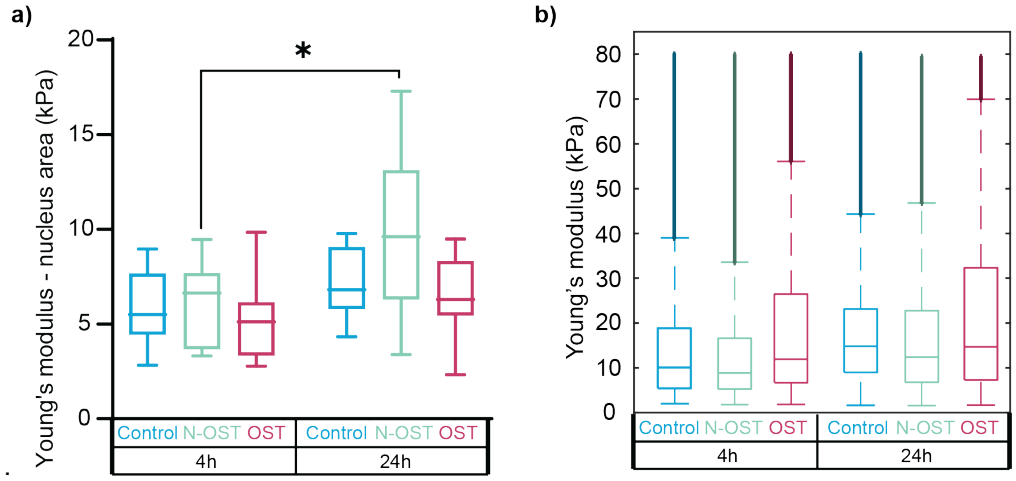


**Figure 9.** (a) Recorded Young's modulus values in the nuclear area of the cells. (b) Overall Young's modulus values recorded in the scanned areas. The plots include all the data points recorded by QI imaging (in the range of 160,000 data points), and thus the representation of outliers, marked as crosses on the graph, resembles a line due to the sheer number of data points. Data points include both information about the cells scanned and information about the Young's modulus of the substrate, especially in the case of submicron patterns. The boxplots in both graphs were created following Tuckey's method. Non-parametric one-way ANOVA (Kruskal-Wallis test) was used to test for statistically significant differences (* $p < 0.016$)

## 3.4. Quantification of cellular adhesion

The results of the adhesion experiments were recorded as force-distance (FD) curves (Figure 10). The FD curves reveal the force of adhesion ($F_{adh}$ – represented by the peak of the curve) and the work of adhesion ($W_{adh}$ – represented by the area between the X-axis and the retract curve) (Figure 10). FDs acquired after an FFM experiment do not generally reveal individual detachment events, that could be expected after consulting FD data recorded by SCFS [19]. The lack of these events can be attributed to the stiffer AFM probe used for FFM (2 N/m) as opposed to the more sensitive SCFS probe (0.03 N/m).

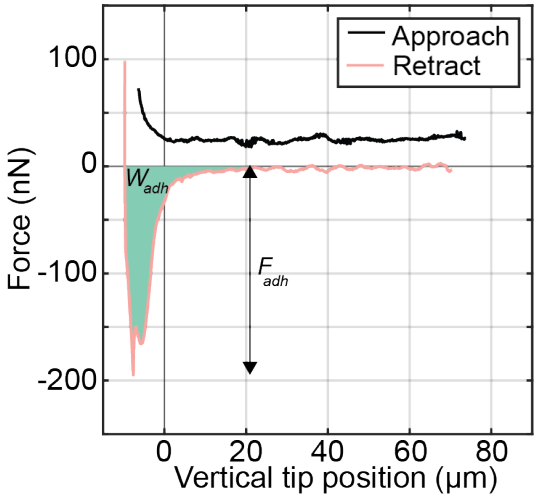


**Figure 10.** Generic FFM FD curve: black curve represents the approach segment of the probe movement, with the indentation of the cell starting at the 0 point on the X-axis, light pink curve represents the retraction part of the probe movement. Peak of retraction curve reveals the maximum $F_{adh}$. Area between the retract curve and the X-axis represents $W_{adh}$.

Cell detachment experiments were conducted mostly within the first 2h after the sample was removed from the incubator (62.5 %), 30.5 % of experiments were conducted between 2h and 3h and 7.0 % of experiments were conducted between 3h and 4h. There was no correlation found in the data between the adhesion properties of the cells and the time they spent in the petri dish heater before they were detached from the surface (please see Appendix J). For each substrate and culture condition, FD curves from 12 different cells have been recorded and analysed. Representative FD curves are included in Figure 11.

***$F_{adh}$*** after **4h** of incubation did not reveal any statistically significant differences between the cells seeded on different substrates (Figure 12a). Moreover, there was no apparent trend for the adhesion force on the three different substrates after 4h of incubation (Figure 12a, Table 3). Likewise, after **24h** of incubation, there were no statistically significant differences between the substrates but a trend can be observed. Cells seeded on the N-OST submicron pattern had a lower $F_{adh}$ than cells on the OST and flat control substrates, and presented the highest standard deviation among the conditions (Figure 12a, Table 3). Regarding the evolution between 4h and 24h, an apparent increasing trend was observed for the $F_{adh}$ for cells seeded on the flat control and the OST submicron pattern (Figure 11 a, Table 3).

***$W_{adh}$*** after **4h** of incubation presented no apparent or statistical differences between the three substrates (Figure 12b, Table 3). After **24h** of incubation, the work of adhesion did not present a

statistically significant difference between the substrates but, as in the case of the force of adhesion, there was a trend present. Cells cultured on the N-OST submicron pattern needed a lower work to be detached than the cells cultured on the flat control and the OST substrates. The latter have similar average values and standard deviations (Figure 12b, Table 3). $W_{adh}$ does not increase for cells seeded on the N-OST submicron pattern between 4h and 24h while there is an increasing trend for the cells present in the other two conditions (Figure 12b, Table 3).

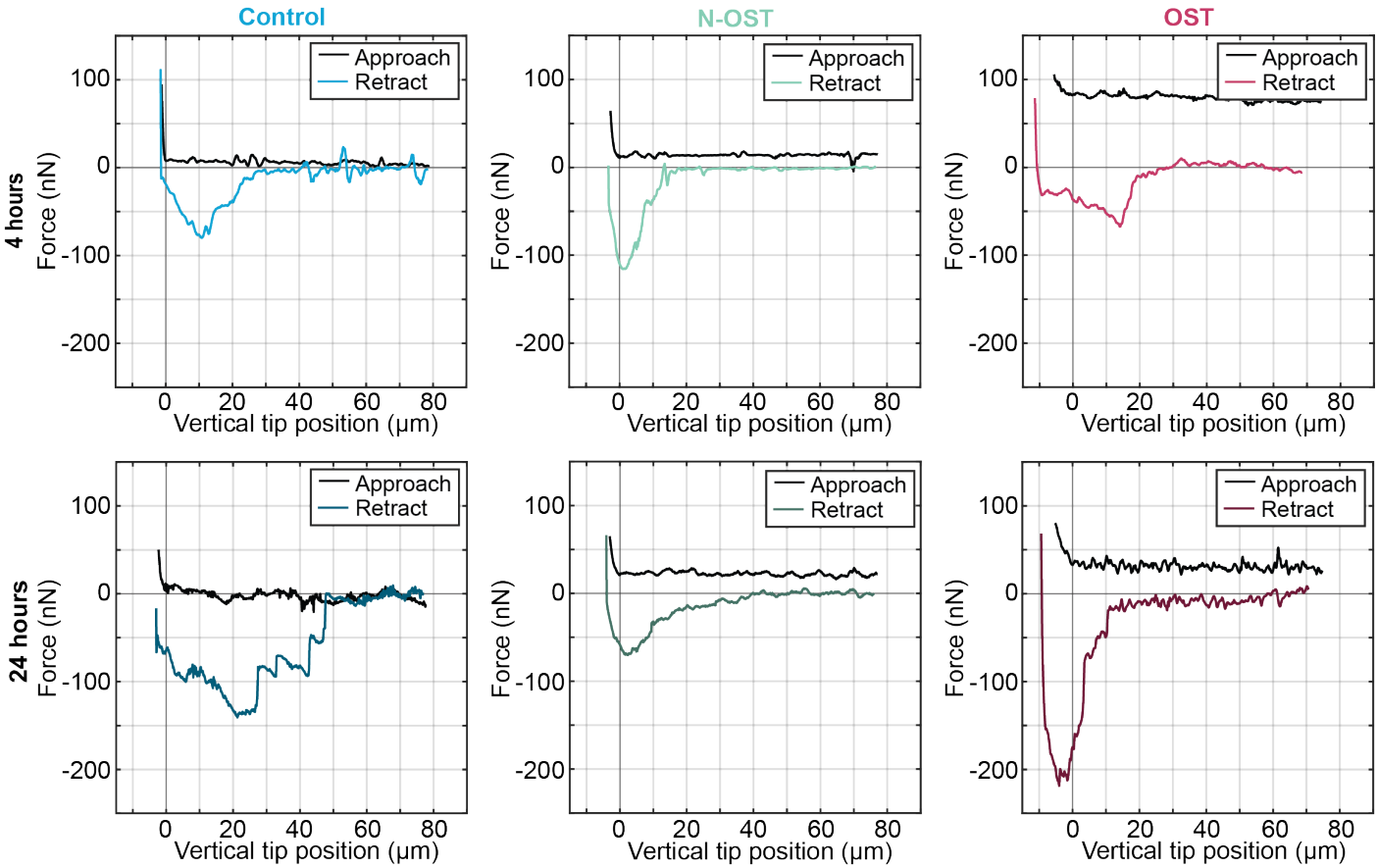


**Figure 11.** Representative FD curves for each condition

**Table 3.** Summary of quantified adhesion properties of cells recorded for each condition (mean ± SD)

| | *Force (nN)* | | *Work (pJ)* | |
|---|---|---|---|---|
| | 4h | 24h | 4h | 24h |
| Control | 87 ± 48 | 161 ± 95 | 0.8 ± 0.41 | 1.99 ± 1.29 |
| N-OST | 84 ± 39 | 108 ± 104 | 1.18 ± 0.58 | 1.04 ± 0.59 |
| OST | 68 ± 37 | 159 ± 74 | 1.05 ± 0.63 | 2.04 ± 1.26 |

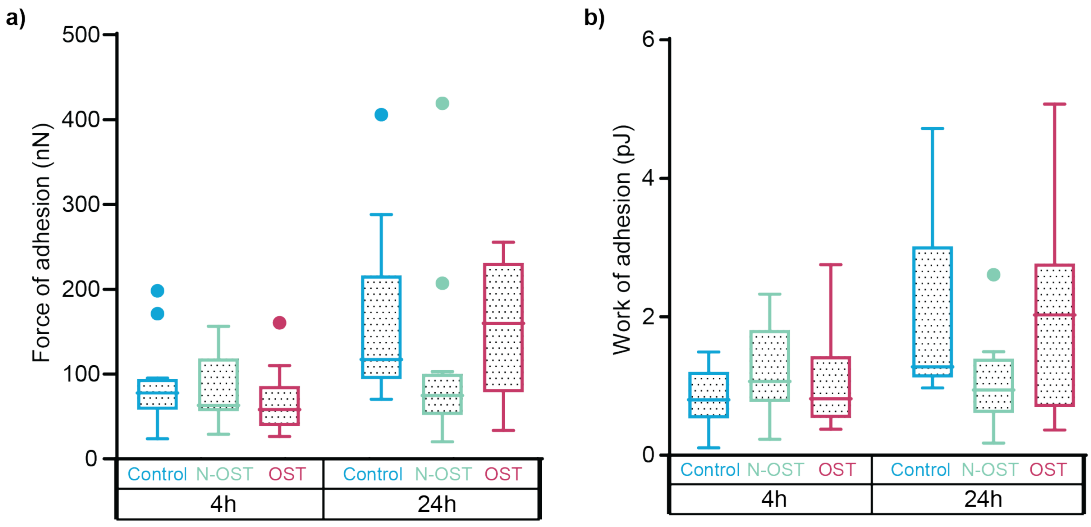


**Figure 12.** Overview of the (a) $F_{adh}$ and (b) $W_{adh}$ for each of the conditions tested. Box plots in both graphs were plotted following Tuckey's method. A non-parametric one-way ANOVA (Kruskal Wallis test) was conducted on the data. No statistically significant differences were found between any of the conditions.

The Spearman rho test revealed statistically significant correlation between the force of adhesion and the work of adhesion in the cases of flat control and the OST submicron pattern, both at 4h (rho = 0.762 for control and rho = 0.811 for OST submicron pattern) and 24h (rho = 0.741 for control and rho = 0.804 for OST submicron pattern) and for the N-OST substrate, only after 24h of incubation (rho = 0.636). No statistically significant correlations between the force and work of adhesion were registered on the N-OST submicron pattern after 4h of cell incubation (rho = 0.315).

In summary, the FFM measurements showed no significant differences in the $F_{adh}$ and $W_{adh}$ after 4 h of cell culture on the two patterns. After 24 h of culture, the trend indicated larger average values for the OST patterns vs N-OST patterns although not statistically significant.

# 4. Discussion

The aim of this work was to assess the adhesion behaviour of preosteoblast cells when cultured on selected submicron patterns, namely an osteogenic (OST) and a non-osteogenic (N-OST). Adhesion is thought to be one of the cellular properties that influences the differentiation of MSC/progenitor cells. Hence, it was of interest to study these cells on the different substrates to possibly identify distinguishing behaviour of cells on the osteogenic pattern relative to the non-osteogenic one.

Therefore, submicron patterns were successfully manufactured to act as cell culture surfaces. Deviations in printed dimensions may be caused by laser power fluctuations or change in the environmental conditions such as room humidity and temperature. Material elastic modulus is in accordance with previously reported material properties, after identical exposure conditions [29]. Taller pillars will deflect more than shorter pillars for the same amount of force applied at the tip (as the force moment is directly proportional with the moment arm [30]). As a consequence, cells may interpret the taller pillars (namely the OST submicron pattern) as a softer substrate than the shorter pillars (N-OST submicron pattern)[10].

The pattern-induced effects on the cellular adhesion properties (*i.e.,* force of adhesion and work of adhesion) were successfully quantified by means of FFM for the first time. After **4 hours** of incubation

there were no noticeable differences between the adhesion properties of cells cultured on the three substrates even though morphological data indicated differences between the evolution of cells (Figure 6). The preferred cell shapes for each substrate indicated that they may be in different stages of adhesion maturation. Cells that adopt an elongated shape, found mainly on the submicron patterns (Figure 7) are considered to be at a more mature adhesion stage than the polygonal cells [31]. Moreover, cells measured on the control substrate spread to areas significantly larger than on the OST substrate without showing an increasing trend in the adhesion force (Figure 12a). Adhesion does not seem to be correlated with the degree of cytoskeleton fiber formation either (Figure 8), as cells cultured on the flat control (cells that developed the best defined fibers after 4h of incubation) did not show different values in $F_{adh}$ or $W_{adh}$ than the cells seeded on the other two substrates (Figure 12).

After **24 hours** of incubation, the adhesion data revealed a trend, even if no statistically significant difference was recorded. Cells seeded on the flat control and the OST substrate (which showed relatively comparable $F_{adh}$ and $W_{adh}$) developed stronger adhesion than the cells incubated on the N-OST substrate (Figure 12). It is interesting to note that the largest and smallest cells presented comparable $F_{adh}$ and $W_{adh}$ (Figure 12). The polarization and the subsequent fibres development in cells seeded on the N-OST pattern did not lead to a change, on average, in adhesion force and adhesion work.

The outliers in the $F_{adh}$ data for cells in the N-OST, after 24h of incubation, exhibited the highest force of adhesion out of all the substrates. These data points ($F_{adh}$ = 420 nN and $F_{adh}$ = 208 nN) were obtained after the detachment of two stellate cells. Likewise, all the cells with $F_{adh}$ > 220 nN (*i.e.,* strongest adherent cells) on the OST pattern (after 24h of incubation) were having a stellate shape. These results are hinting that stellate cells, that were mostly observed on the OST patterns having the taller pillars, may develop a stronger adhesion with the underlying substrate than cells that develop elongated or polygonal morphologies.

Regarding the evolution of cellular properties between the two time points investigated, cells cultured on the OST submicron pattern showed an apparent increase in both adhesion force and adhesion work (Figure 12) but no observable changes in the degree of fibres formation (Figure 8). Following opposite trends, cells on the N-OST patterns presented similar adhesion properties after both 4h and 24h of incubation (Figure 12) but the N-OST pattern was the only substrate to induce an increase in the formation of fibres (Figure 8). This aspect was also reflected in the increase in the average Young's modulus in the nuclear region of these cells (Figure 9 a). Cells cultured on flat control presented a stronger bond with the substrate at 24h than at 4h but showed no observable changes in the degree of fibre formation. These observations come to support the fact that the degree of fibre formation is not related to the adhesion properties of the cells.

A correlation was observed however between the $F_{adh}$ and $W_{adh}$. This finding indicates that once the cell – substrate bond starts to break (recorded as the peak of the retract curve -Figure 11), the detachment occurs gradually. Video recordings of cell detachment experiments show how, as the probe retracts, the peripheric regions of the cell were the last ones to break away from the substrate (videos will be available at repository.tudelft.nl/). The correlation may suggest that if the cell develops strong adhesion patches near the nuclear region (*i.e.,* the first bonds to break), all the adhesion structures formed throughout the cells are similar in nature and strength.

The different degrees of fibre formation do not seem to be reflected in the overall comparison of the Young's modulus of cells (Figure 9b). On one hand, the measurement can not identify the different

contributors to the overall stiffness of the cells (histogram visualization of the data may be more suitable for this purpose – Appendix K). On the other hand, the patterns induce noise in the higher end of the Young's modulus measured range (namely between 40 and 80 kPa) and thus artificially increase the average Young's modulus of the cells. Cells scanned on stiffer substrates can be isolated better as most of the data points acquired on the substrates around the cells have a Young's modulus of over 80 kPa.

The surface induced differences in cellular evolution may be accounted for by the differences between substrate properties. The increase in height of pillars (and thus in roughness) hinders cellular spread which in turn leads to a decreased in the degree of fibres formation [12]. This observation was also reported in previous work investigating the effects of submicron structures on cellular evolution [10,12]. The extent of cell spread can be linked to the available potential ligation points between the cell and the substrate. If glass offers a virtually infinite number of ligation points, patterns discretize the interaction sites [12]. Nouri-Goushki *et al* [10] (working with similarly designed patterns) reported that cells only adhered to the tips of the OST pillars, while on the N-OST pillars cells also adhere to the sides and even underlying glass surface at the periphery.

Moreover, the adhesion strength seems to have increased with the increase in the pillars' height. Increasing the degree of discretization of ligation points seems to lead to a different organization of intracellular adhesion related structures (such as focal adhesion sites). This aspect can also explain the similar adhesion strength between cells cultured on the flat control and the OST submicron pattern: area of the contact patch (*i.e.*, area that takes the stress induced by the detachment experiment) between the cell and the substrate may be similar between the cells coming from the two different conditions. This hypothesis is supported by previous findings: Goushki *et al* [10], Niepel *et al* [12] and Gonzales *et al* [32] all reported a larger contact patch area (they investigated focal adhesion sites in these studies) within the cells found on patterns offering fewer possible ligation points.

Only one comparable study, using the FFM experimental set up to detach cells, was found in the literature. Wysotzki *et al* [22] investigated similar experimental conditions (identical cell types, incubated on a glass surface for 24h) but found an average $F_{adh}$ and $W_{adh}$ in the range of 500 nN and 12 pJ respectively (*i.e.,* approximately 5 times higher than the values reported in this study for the flat control). The experimental difference was the probe moving speed, 5 μm/s (as opposed to 1 μm/s reported here). This suggests that the viscoelastic properties of cells play a role in the recorded adhesion values during a detachment experiment.

# 5. Conclusions

The adhesion is thought to play an important role in the differentiation of multipotent cells and thus a better understanding of the cellular adhesion properties may enable engineers to develop implants that can beneficially direct cells behaviour. One such field, where this understanding could be important, is represented by the orthopaedic implants which could benefit from implant surfaces that can lead to better and faster osseointegration. Nano and submicron physical patterns have been proven effective in promoting osteogenic differentiation of MSCs and progenitor cells. Nevertheless, until now, cells' adhesion was characterized only in qualitative ways, with no hard quantified information about the evolution of adhesion. Moreover, the quantification of adhesion data may offer a novel biomarker to be used to determine the differentiation path a cell is undergoing, at a much earlier time point than the conventional tests.

In this study, the adhesion of preosteoblast cells was successfully quantified on two types of submicron pattern with known osteogenic potential, and compared to cellular adhesion data on a flat control. Therefore, the fluid force microscopy (FFM) was applied for the first time. Cells seeded on the osteogenic (OST) substrate adhered stronger than cells on the non-osteogenic (N-OST) substrate after 24h of incubation. The difference was not statistically significant but the trend was present. The data also hints at a correlation between the cell shape and the strength of adhesion, with stellate cells appearing to develop a stronger adhesion with the substrate (the data is however scarce at this point).

No correlation was noticed between the degree of fibres formation within the cells and the strength of adhesion. Although cells cultured on the OST pattern generally did not show a visible increase in the amount of intracellular fibres between 4h and 24h, the data showed an increasing trend in the adhesion strength. In the same time, scanning of cells in the N-OST conditions revealed an increase in the amount of formed fibres from 4h to 24h but the average $F_{adh}$ and $W_{adh}$ remained relatively constant.

Preosteoblasts adopted a specific morphology and seemed to adhere stronger on the taller pillars, suggesting that a stronger adhesion may be characteristic for cells that undergo osteogenic differentiation. It is, however, too early to rely on adhesion tests as biomarkers for the osteogenic differentiation. Nevertheless, the FFM method has been proven as a powerful tool to quantify the adhesion properties of cells on submicron pillars. The information presented here open the door for further investigations.

# 6. Future work

An aspect that may reinforce the findings presented here is conducting more detachment experiments for the six conditions presented here. Besides strengthening the conclusions and reducing the influence of outliers, additional data points may allow for a more accurate comparison between adhesion properties of cells of different morphologies (polygonal vs stellate vs polarized). A stronger data base of adhesion properties of cells on the three different substrates may allow for further investigations into how FFM methodology can be improved.

FFM is still in the early phase of being employed in cell detachment and thus its full understanding is crucial for it to be employed at its maximum capacity. As seen in previous work [22], the speed of probe movement can have a significant impact on the recorded adhesion data. A first step should be to test the correlation between this speed and the recorded data. This understanding could potentially be used to tune the probe movement speed so that the recorded differences in adhesion between different conditions becomes more apparent and relevant.

Adhesion data is not all that should be taken into account with these substrates-induced cellular changes. The scanning of the entire cell does not seem to reveal enough information in relation to the adhesion information. Firstly, a better processing algorithm for the mechanical maps may filter the noise better and thus avoid any influence from the substrates in the cell comparisons. Secondly, scanning key areas on a cell (like nucleus or membrane protrusions) may reveal more relevant information about the state of the cell. Scanning a smaller area on the cell may reveal details not otherwise sensed by the AFM probe.

Moreover, coupling the adhesion data with fluorescence microscopy experiments may help reveal the nature of fibres being formed by the cells in the three different conditions. Taking fluorescence microscopy a step further, live staining of cellular structures (*e.g.,* actin filaments, vinculin) may enable their imaging prior to a detachment experiment. Even more interesting, live cell staining may enable the tracking of the intracellular structures as they move and rearrange as the bond between the cell and the substrate is breaking.

# References


[1] R. Agarwal, A.J. García (2015), Biomaterial strategies for engineering implants for enhanced osseointegration and bone repair, Advanced Drug Delivery Reviews, 94, 53-62 . https://doi.org/10.1016/j.addr.2015.03.013.

[2] F. Barrère, T.A. Mahmood, K. de Groot, C.A. van Blitterswijk (2008), Advanced biomaterials for skeletal tissue regeneration: Instructive and smart functions, Materials Science and Engineering R: Reports, 59, 38-71. https://doi.org/10.1016/j.mser.2007.12.001.

[3] Dutch Arthroplasty Register, LROI Annual Report 2018, 2019.

[4] S. Dobbenga, L.E. Fratila-Apachitei, A.A. Zadpoor (2016), Nanopattern-induced osteogenic differentiation of stem cells – A systematic review, Acta Biomaterialia, 46, 3-14. https://doi.org/10.1016/j.actbio.2016.09.031.

[5] Y.K. Wang, C.S. Chen (2013), Cell adhesion and mechanical stimulation in the regulation of mesenchymal stem cell differentiation, Journal of Cellular and Molecular Medicine, 17, 823-832. https://doi.org/10.1111/jcmm.12061.

[6] M.M. Stevens, J.H. George (2005), Exploring and engineering the cell surface interface, Science, 310, 1135-1138. https://doi.org/10.1126/science.1106587.

[7] R.K. Das, O.F. Zouani (2014), A review of the effects of the cell environment physicochemical nanoarchitecture on stem cell commitment, Biomaterials, 35, 5278-5239. https://doi.org/10.1016/j.biomaterials.2014.03.044.

[8] K. Ye, L. Cao, S. Li, L. Yu, J. Ding (2016), Interplay of Matrix Stiffness and Cell-Cell Contact in Regulating Differentiation of Stem Cells, ACS Applied Materials and Interfaces, 8, 21903-21913. https://doi.org/10.1021/acsami.5b09746.

[9] M.J. Dalby, N. Gadegaard, R. Tare, A. Andar, M.O. Riehle, P. Herzyk, C.D.W. Wilkinson, R.O.C. Oreffo (2007), The control of human mesenchymal cell differentiation using nanoscale symmetry and disorder, Nature Materials, 6, 997-1003. https://doi.org/10.1038/nmat2013.

[10] M. Nouri-goushki, L. Angeloni, K. Modaresifar, M. Minneboo, P. Boukany, M. Mirzaali, M. Ghatkesar, L.E. Fratila-Apachitei, A.A. Zadpoor, 3D printed submicron patterns reveal the interrelation between cell adhesion , cell mechanics , and osteogenesis, Submitted for Publication (n.d.) 1–42.

[11] H.L. Khor, Y. Kuan, H. Kukula, K. Tamada, W. Knoll, M. Moeller, D.W. Hutmacher (2007), Response of cells on surface-induced nanopatterns: Fibroblasts and mesenchymal progenitor cells, Biomacromolecules, 8, 1530-1540. https://doi.org/10.1021/bm0611533.

[12] M.S. Niepel, B. Fuhrmann, H.S. Leipner, T. Groth (2013), Nanoscaled surface patterns influence adhesion and growth of human dermal fibroblasts, Langmuir, 29, 13278-13290. https://doi.org/10.1021/la402705r.

[13] S. Lavenus, M. Berreur, V. Trichet, P. Pilet, G. Louarn, P. Layrolle (2010), Adhesion and

osteogenic differentiation of human mesenchymal stem cells on titanium nanopores, European Cells and Materials, 22, 84-96. https://doi.org/10.22203/eCM.v022a07.

[14] F.P.W. Melchels, M.A.N. Domingos, T.J. Klein, J. Malda, P.J. Bartolo, D.W. Hutmacher (2012), Additive manufacturing of tissues and organs, Progress in Polymer Science, 37, 1079-1104. https://doi.org/10.1016/j.progpolymsci.2011.11.007.

[15] D.S. Engstrom, B. Porter, M. Pacios, H. Bhaskaran (2014), Additive nanomanufacturing - A review, Journal of Materials Research, 29, 1792-1816. https://doi.org/10.1557/jmr.2014.159.

[16] M.J. Sanderson, I. Smith, I. Parker, M.D. Bootman (2014), Fluorescence microscopy, Cold Spring Harbor Protocols, 10. https://doi.org/10.1101/pdb.top071795.

[17] K.W. Kwon, S.S. Choi, B. Kim, S.N. Lee, M.C. Park, P. Kim, S.H. Lee, S.H. Park, K.Y. Suh (2006), A microfluidic flow sensor for measuring cell adhesion, in: 2006 5th IEEE Conference on Sensors, 105-108. https://doi.org/10.1109/ICSENS.2007.355729.

[18] C. V Sapan, R.L. Lundblad, N.C. Price (1999), Colorimetric protein assay techniques., Biotechnology and Applied Biochemistry, 29. https://doi.org/10.1111/j.1470-8744.1999.tb00538.x.

[19] J. Friedrichs, K.R. Legate, R. Schubert, M. Bharadwaj, C. Werner, D.J. Müller, M. Benoit (2013), A practical guide to quantify cell adhesion using single-cell force spectroscopy, Methods, 60, 169-178. https://doi.org/10.1016/j.ymeth.2013.01.006.

[20] E. Potthoff, O. Guillaume-Gentil, D. Ossola, J. Polesel-Maris, S. LeibundGut-Landmann, T. Zambelli, J.A. Vorholt (2012), Rapid and Serial Quantification of Adhesion Forces of Yeast and Mammalian Cells, PLoS One, 7. https://doi.org/10.1371/journal.pone.0052712.

[21] T. Naganuma (2017), The relationship between cell adhesion force activation on nano/micro-topographical surfaces and temporal dependence of cell morphology, Nanoscale, 9, 13171-13186. 13171–13186. https://doi.org/10.1039/c7nr04785a.

[22] P. Wysotzki, A. Sancho, J. Gimsa, J. Groll (2020), A comparative analysis of detachment forces and energies in initial and mature cell-material interaction, Colloids Surfaces B Biointerfaces, 190, 110894. https://doi.org/10.1016/j.colsurfb.2020.110894.

[23] S. Belikov, J. Alexander, C. Wall, I. Yermolenko, S. Magonov, I. Malovichko (2014), Thermal tune method for AFM oscillatory resonant imaging in air and liquid Thermal Tune Method for AFM Oscillatory Resonant Imaging in Air and Liquid, in: 2014 American Control Conference, Portland, OR, 1009-1014. https://doi.org/10.1109/ACC.2014.6859224.

[24] Bruker Corporation (2005). The NanoWizard ® AFM Handbook, retrieved from https://bc-uu.nl/cci/wp-content/uploads/2014/01/JPK-handbook.1.3.pdf.

[25] L. Jaatinen, E. Young, J. Hyttinen, J. Vörös, T. Zambelli, L. Demkó (2016), Quantifying the effect of electric current on cell adhesion studied by single-cell force spectroscopy, Biointerphases, 11, 11004. https://doi.org/10.1116/1.4940214.

[26] Cytosurge (2020). FluidFM ® add-on from Cytosurge Instructions.

[27] M. Sztilkovics, T. Gerecsei, B. Peter, A. Saftics, S. Kurunczi, I. Szekacs, B. Szabo, R. Horvath (2020), Single-cell adhesion force kinetics of cell populations from combined label-free optical biosensor and robotic fluidic force microscopy, Scientific Reports, 10. https://doi.org/10.1038/s41598-019-56898-7.

[28] X. Zhou, Y. Hou, J. Lin (2015), A review on the processing accuracy of two-photon polymerization, AIP Advances, 5, 30701. https://doi.org/10.1063/1.4916886.

[29] M. Nouri-Goushki, A. Sharma, L. Sasso, S. Zhang, B.C.J. Van Der Eerden, U. Staufer, L.E. Fratila-Apachitei, A.A. Zadpoor (2019), Submicron Patterns-on-a-Chip: Fabrication of a Microfluidic Device Incorporating 3D Printed Surface Ornaments, ACS Biomaterials Science and Engineering, 5, 6127-6136. https://doi.org/10.1021/acsbiomaterials.9b01155.

[30] J.L. Meriam, L.G. Kraige, Engineering mechanics Volume 1 Statics, 7th ed., John Wiley & Sons, Inc., 2006.

[31] N.C. Gauthier, T.A. Masters, M.P. Sheetz (2012), Mechanical feedback between membrane tension and dynamics, Trends Cell Biology, 22, 527-535. https://doi.org/10.1016/j.tcb.2012.07.005.

[32] C. González-García, S.R. Sousa, D. Moratal, P. Rico, M. Salmerón-Sánchez (2010), Effect of nanoscale topography on fibronectin adsorption, focal adhesion size and matrix organisation, Colloids Surfaces B Biointerfaces, 77, 181-190. https://doi.org/10.1016/j.colsurfb.2010.01.021.

[33] Newport Corporation, Application note. Three-Dimensional Microfabrication by Two-Photon Polymerization, retrieved from: https://www.newport.com/medias/sys_master/images/images/h26/hf7/8797287743518/Three-Dimensional-Microfabrication-App-Note-37.pdf

[34] A. Rigato, F. Rico, F. Eghiaian, M. Piel, S. Scheuring (2015), Atomic Force Microscopy Mechanical Mapping of Micropatterned Cells Shows Adhesion Geometry-Dependent Mechanical Response on Local and Global Scales, ACS Nano, 9, 5846-5856. https://doi.org/10.1021/acsnano.5b00430.

**Table of Figures**

**List of tables**

# Supplementary materials

## A. DeScribe code for submicron pattern generation

```
%Same code can be used for both P2 and P3
% There are 2 files 2 in the folder: stlH_1200 and stlH_1900
%   stlH stands for STL height
%    Change between stlH_1200 (=P2) and stlH_1900 (=P3)
InvertZAxis 0
% Writing configuration
GalvoScanMode
ContinuousMode
Recalibrate
Resetinterface
PiezoSettlingTime 10
GalvoAcceleration 2
StageVelocity 200
local $i = 0
local $k = 0
local $j = 0
local $m = 0
XOffset 0
YOffset 0
StageGotoX 0
StageGotoY 0
%Print marker in the center of the glass slide
CenterStage
LaserPower 18
ScanSpeed 1200
var $interfacePos = 0.2
InterfaceAccuracyHigh
include sign 2by5_data.gwl
MoveStageX 30
InterfaceAccuracyHigh
include sign 2by5_data.gwl
MoveStageY 30
InterfaceAccuracyHigh
include sign 2by5_data.gwl
MoveStageY -60
InterfaceAccuracyHigh
include sign 2by5_data.gwl
MoveStageX -30
InterfaceAccuracyHigh
include sign 2by5_data.gwl
MoveStageY -30
InterfaceAccuracyHigh
include sign 2by5_data.gwl
% Move pattern 2mm to the right
```

```
CenterStage
   var $interfacePos = 0.2
   MoveStageX 2700
% Print 1x1 mm pattern
   for $i=1 to 25
      for $j = 1 to 25
         LaserPower 14
         ScanSpeed 1200
         InterfaceAccuracyHigh
         FindInterfaceAt 0.2
         % Include slicer output
         include stlH1900_data.gwl
         XOffset 0
         YOffset 0
         MoveStageX 40
         MoveStageY 0
      end
      XOffset 0
      YOffset 0
      MoveStageX -1000
      MoveStageY 40
   End
```

## B. Height map processing MATLAB code

```
close all
clear

% Define the number of file paths you want to analyze
num_conditions = input('How many conditions you want to anayse? ');

for i = 1:num_conditions

% For each file path, find the text files and extract the numerical data
    directory_name = input('Input path for text files ', 's');
    cd(directory_name)

    Files = dir('*.txt');
    num_datasets = length(Files);

    for k = 1:num_datasets

       file_name = Files(k).name;
       fid = fopen(file_name, 'r');
       if fid == -1
        error('Cannot open file fpr reading: %s', FileName);
       end

        DataC = textscan(fid, '%s', 'delimiter', '\n', 'whitespace', '');
        data  = DataC{1};
        fclose(fid);

        index_pause = find(contains(data, '# segmentIndex: 1'));
        index_retract = find(contains(data, '# segmentIndex: 2'));

        data(index_pause:(index_retract-1)) = [];
        data(find(contains(data, '#'))) = [];
        data(data == "") = [];
        data_numeric = str2num(char(data(:)));

        dt_um = data_numeric .* 10^6;

%Plot the numerical data found within each text file

        h1 = figure('Renderer', 'painters', 'Position', [10 10 900 900]);
        map = pcolor(dt_um);
        colormap(hot)
        c = colorbar;
        c.Label.String = 'Height (\mum)';
        caxis([0 1])
        set(gca,'FontSize',20)
        xlabel({'um'},'fontsize', 24);
        ylabel({'um'},'fontsize', 24);
        title({['cell0',num2str(k)]})
    end

end
```

## C. Cell culture protocols

| *CCB training protocol no.: 3* | *Revision no.: 000* | *Date: 7 november 2018* |
|---|---|---|
| **Cell seeding pre culture** | | |

1. Requirements

1.1 Equipment
- 1.5 ml tube
- 50ml tubes
- P20 pipette + filter tips
- P1000 pipette + filter tips
- 5ml plastic pipettes
- 10ml plastic pipettes
- Suction system
- Water bath at 37°C
- 50ml tube centrifuge (sigma centrifuge)

1.2 Reagents
-Culture medium

1.3 Cells
- 1 vial frozen cells

2. Procedure

2.1 Protocol
1. Fil 1 50ml tube with 10ml of culture medium.
2. Take 1 vial with cells from the -80.
3. Directly put the vial in the water bath, watch the vial closely and remove as soon as the last sliver of ice melts. **Hold the vial during this step, do not put it completely under water.**
4. Wipe vial with ethanol before placing it in the biosafety cabinet.
5. Pipet the cells with the P1000 pipette into the 50 ml tube. Rinse the vial 2 times with 1 ml medium and add to the same 50 ml tube.
6. Adjust the volume of medium to 25ml.
7. Spin down for 5 minutes at 200 x g.
8. Carefully remove the supernatant by using the suction system.
9. Resuspend the cells in 1ml medium by pipetting up and down until no clumps of cells are visible anymore.
10. Transfer 2 samples of 10µl each into a 1.5ml tube to count the amount of cells (see protocol 4).
11. Seed $5x10^5$ viable cells per 75 $cm^2$ flask in 10 ml medium.
12. Distribute cells evenly by moving the flask quickly according to a cross-like pattern.
13. Transfer flask into a $CO_2$ incubator (37°C, 5% $CO_2$).
14. Replace the medium every 2 to 3 days: Remove medium from flask carefully by using the suction system. Add 10ml pre warmed medium.
15. Keep the cells in pre-culture for 7 days until confluence is reached.

| *CCB Training protocol no.: 4* | *Revision no.: 000* | *Date: 7 november 2018* |
|---|---|---|
| **Cell counting** | | |

1. Requirements

1.1 Equipment
- 1.5 ml tubes
- P20 pipet + tips
- Counting slides (Biorad 145-0011)
- Cell counter (Biorad TC20 cell counter)

1.2 Reagents
- Trypan blue (Biorad #145-0021)

2. Procedure

For this protocol the TC20 cell counter will be used.
Switch on the machine before starting the counting procedure.

2.1 Protocol

1. Pipet 10µl of the cell suspension into a 0.5ml tube (in duplo)
2. Pipet 10µl of trypan blue dye into the same 1.5ml tube and mix gently by pipetting up and down 10 times. **Do not vortex.**
3. Pipet 10µl of the mixture into the opening of one chamber on the counting slide. **When loading the slide, place the pipet tip at a 45° angle.**
4. Insert the counting slide into the slide slot of the TC20 cell counter. The machine will automatically initiate a cell count. **Make sure that the slide is completely inside the slide slot.**
5. The count results appear on the screen: Total cell count per ml, live cell count per ml, and percentage of live cells. **Write down the numbers in your lab journal.**
6. Once the instrument completes the cell count, remove the slide from the slide slot.
7. When finished with counting, discard the counting slide into the biological waste bin.

| *CCB training protocol no.: 5* | *Revision no.: 000* | *Date: 7 november 2018* |
|---|---|---|
| **Cell seeding for experiment** | | |

1. Requirements

1.1 Equipment
- 1.5 ml tube
- 50ml tubes
- P20 pipette + filter tips
- P1000 pipette + filter tips
- Well plates
- 5ml plastic pipettes
- 10ml plastic pipettes
- Suction system
- 50ml tube centrifuge (sigma centrifuge)

1.2 Reagents
- Preheated culture medium
- Preheated 1x Trypsin-EDTA (Thermo fisher # 10779413)
- PBS (Thermo Fisher #14200083)

1.3 Cells
- Pre cultured T75 flask

2. Procedure

2.1 Protocol
1. Remove medium from flask carefully by using the suction system.
2. Wash the cells twice with 10 ml PBS. **Make sure to not add the solution directly onto the cell layer.**
3. Remove PBS from flask carefully by using the suction system.
4. Add 1ml trypsin dropwise on top of the cell layer. Move the flask to distribute the drops over the complete cell layer. Put flask into the incubator.
5. Check after 5 minutes under the microscope whether the cells have already detached from the bottom of the flask,(the cells should be round shaped by this time).
6. Add 10 ml preheated medium to the flask, move the flask gently and transfer the cell suspension to a clean 50ml tube. Repeat this with another 10 ml preheated medium and add to the same tube. Adjust the volume to 25ml with medium.
7. Centrifuge for 5 minutes at 200 x g.
8. Carefully remove the supernatant by using the suction system.
9. Resuspend cell pellet in 1ml preheated medium by pipetting up and down until no clumps of cells are visible anymore.
10. Transfer 2 samples of 10µl each into a 1.5ml tube to count the amount of cells (see protocol 6).
11. Seed appropriate amount of cells for the experiment needed (see table…).
12. Distribute cells evenly by moving the plate quickly according to a cross-like pattern.
13. Incubate the plate for 2 days in a $CO_2$ incubator (37°C, 5% $CO_2$).

## D. Young's modulus maps and individual histogram plotting

```
close all
clear

num_bins = 200; % number of beans used for histogram plotting
num_conditions = input('How many conditions you want to anayse? ');
fit_out = zeros(num_conditions);
mean_x = zeros(num_conditions);
x = linspace(2000, 80000, num_bins+1);

set(0,'DefaultFigureVisible','on');

for idx = 1:num_conditions

    directory_name = input('Input path for text files ', 's');

    %Plot Young's modulus colour maps for all the text files present in one directory.
    %The function will also plot a rough set of histograms for each
    %individual cell and the avergaed histograms per conditions. These
    %histograms were not used for data anlysis.
    [avg_count, avg_edg] = h_batch(directory_name, num_bins);

    figure();
    bar(avg_edg(1:end-1), avg_count);
    xlabel({'Young''s modulus (Pa)'},'fontsize', 10);
    ylabel({'Count'},'fontsize', 10);
    set(gca,'FontSize',10)
    xlim([0 80000])
    ylim([0 2.5])
    x0=10;
    y0=10;
    width = 600;
    height = 600;
    set (gcf, 'position', [x0,y0,width,height])
    grid on;
    title ({['Average histogram']})

    [avg_fit_g3, gof] = createFit_gauss3(avg_edg(1:end-1), avg_count);
    xlabel({'Young''s modulus (Pa)'},'fontsize', 10);
    ylabel({'Count'},'fontsize', 10);
    set(gca, 'FontSize', 10)
    xlim([0 80000])
    ylim([0 2.5])
    x0=10;
    y0=10;
    width = 600;
    height = 600;
    set (gcf, 'position', [x0,y0,width,height])
    title ({'Condition: '})
    hold on

    fit_data = avg_fit_g3(x);
    fit_out(idx) = median(avg_count);
    [bla, mean_pos] = min(abs(avg_count - fit_out(idx)));
    median_x(idx) = x(find(avg_count(mean_pos)));
end

hold off

%% Function definition
```

```
%% JPK files processing

function [avg_counts, avg_edg] = h_batch(directory_name, num_bins)

    set(0,'DefaultFigureVisible','on');

    cd(directory_name)

    Files = dir('*.txt');
    num_datasets = length(Files);
    hist_x = zeros(num_datasets, num_bins);
    hist_y = zeros(num_datasets, num_bins);
    edges = linspace(2000, 80000, num_bins+1);
    numedges = num_bins+1;
    counts = zeros(numedges-1, num_datasets);
    edg = zeros(num_bins+1, num_datasets);

    for k = 1:length(Files)
       file_name = Files(k).name;
       fid = fopen(file_name, 'r');
       if fid == -1
        error('Cannot open file fpr reading: %s', FileName);
       end

        DataC = textscan(fid, '%s', 'delimiter', '\n', 'whitespace', '');
        data  = DataC{1};
        fclose(fid);

        index_pause = find(contains(data, '# segmentIndex: 1'));
        index_retract = find(contains(data, '# segmentIndex: 2'));

        data(index_pause:(index_retract-1)) = [];
        data(find(contains(data, '#'))) = [];
        data(data == "") = [];
        data_numeric = str2num(char(data(:)));

        data_numeric(data_numeric < 2000) = 0;
        data_numeric(data_numeric > 80000) = 0;

        non_zero_data = data_numeric(data_numeric ~= 0);

        data_numeric(data_numeric == 0) = NaN;
        non_zero_data = log10(non_zero_data);

        set(0,'DefaultFigureVisible','off');

        h1 = figure('Renderer', 'painters', 'Position', [10 10 600 600]);
        pcolor(data_numeric);
        c = colorbar;
        c.Label.String = 'Pa';
        set(gca,'FontSize',10)
        xlabel({'um'},'fontsize', 10);
        ylabel({'um'},'fontsize', 10);
        title({['cell0',num2str(k)]})
        set(gca, 'FontName', 'Arial')
        %saveas(h1,sprintf('map_cell0%d.png',k));

        [counts(:, k), edg(:, k)] = histcounts(non_zero_data, num_bins); %,
'Normalization', 'countdensity');

        h = figure('Renderer', 'painters', 'Position', [10 10 600 600]);
        [hist_x(k,:), hist_y(k,:)] = histogram(non_zero_data, num_bins);
```

```
        histogram(non_zero_data, num_bins);
        xlabel({'Young''s modulus (Pa)'},'fontsize', 10);
        ylabel({'Count'},'fontsize', 10);
        set(gca,'FontSize',10)
        xlim([0 80000])
        ylim([0 2500])
        set(gca, 'FontName', 'Arial')
        title({['cell0',num2str(k)]})
        %saveas(h,sprintf('cell0%d.png',k));

       set(0,'DefaultFigureVisible','on');
    end

    avg_counts = mean(counts.');
    avg_edg = mean(edg.');
    figure();
end


function [fitresult, gof] = createFit_gauss2(hist_y, hist_x)
%CREATEFIT(HIST_Y,HIST_X)
%  Create a fit.
%
%  Data for 'untitled fit 1' fit:
%      X Input : hist_y
%      Y Output: hist_x
%  Output:
%      fitresult : a fit object representing the fit.
%      gof : structure with goodness-of fit info.
%
%  See also FIT, CFIT, SFIT.

%  Auto-generated by MATLAB on 16-Oct-2020 12:32:52


%% Fit: 'Gauss fit 2'.
[xData, yData] = prepareCurveData( hist_y, hist_x );

% Set up fittype and options.
ft = fittype( 'gauss2' );
opts = fitoptions( 'Method', 'NonlinearLeastSquares' );
opts.Display = 'Off';
opts.Lower = [-Inf -Inf 0 -Inf -Inf 0];
opts.StartPoint = [1827 3672.34267896925 4745.38287051949 777.385930190775
12586.3634967531 5584.58342665932];

% Fit model to data.
[fitresult, gof] = fit( xData, yData, ft, opts );

% Plot fit with data.
figure( 'Name', 'untitled fit 1' );
h = plot( fitresult, xData, yData );
legend( h, 'Histogram', 'Gauss fit 2', 'Location', 'NorthEast', 'Interpreter', 'none'
);
xlim([0 80000])
ylim([0 500])
% Label axes
xlabel( 'hist_y', 'Interpreter', 'none' );
ylabel( 'hist_x', 'Interpreter', 'none' );

grid on
```

```
end

function [fitresult, gof] = createFit_gauss3(hist_y, hist_x)
%CREATEFIT(HIST_Y,HIST_X)
%  Create a fit.
%
%  Data for 'gauss fit 3' fit:
%      X Input : hist_y
%      Y Output: hist_x
%  Output:
%      fitresult : a fit object representing the fit.
%      gof : structure with goodness-of fit info.
%
%  See also FIT, CFIT, SFIT.

%  Auto-generated by MATLAB on 16-Oct-2020 12:39:23


%% Fit: 'gauss fit 3'.
[xData, yData] = prepareCurveData( hist_y, hist_x );

% Set up fittype and options.
ft = fittype( 'gauss3' );
opts = fitoptions( 'Method', 'NonlinearLeastSquares' );
opts.Display = 'Off';
opts.Lower = [-Inf -Inf 0 -Inf -Inf 0 -Inf -Inf 0];
opts.StartPoint = [1827 3672.34267896925 3163.58858034633 967.804114974817
9243.60569008418 3594.42058148721 509.407811302973 14814.8687011991 4353.69726186199];

% Fit model to data.
[fitresult, gof] = fit( xData, yData, ft, opts );

% Plot fit with data.
figure( 'Name', 'gauss fit 3' );
h = plot( fitresult, xData, yData );
legend( h, 'hist_x vs. hist_y', 'gauss fit 3', 'Location', 'NorthEast', 'Interpreter',
'none' );
xlim([0 80000])
ylim([0 500])
% Label axes
set(gca, 'FontName', 'Arial')
set(gca,'FontSize',10)
xlabel( 'hist_y', 'Interpreter', 'none' );
ylabel( 'hist_x', 'Interpreter', 'none' );
grid on

end
```

## E. Young's modulus data analysis per condition

```
close all
clear

num_bins = 100; %Define the number of bins used for the histograms
num_conditions = input('How many conditions you want to anayse? ');
fit_out = zeros(num_conditions);
mean_x = zeros(num_conditions);
x = linspace(2000, 80000, num_bins+1);

set(0,'DefaultFigureVisible','on');

for idx = 1:num_conditions

    directory_name = input('Input path for text files ', 's');

    [mean_d, std_d] = h_batch(directory_name, num_bins);
end

%% Function definition
%% JPK files processing

function [mean_d, std_d] = h_batch(directory_name, num_bins)

    set(0,'DefaultFigureVisible','on');

    cd(directory_name)

    Files = dir('*.txt');
    data_numeric = zeros(256, 256);

    for k = 1:length(Files)

        %For each file, extract numerical values

       file_name = Files(k).name;
       fid = fopen(file_name, 'r');
       if fid == -1
        error('Cannot open file fpr reading: %s', FileName);
       end

        DataC = textscan(fid, '%s', 'delimiter', '\n', 'whitespace', '');
        data  = DataC{1};
        fclose(fid);

        index_pause = find(contains(data, '# segmentIndex: 1'));
        index_retract = find(contains(data, '# segmentIndex: 2'));

        data(index_pause:(index_retract-1)) = [];
        data(find(contains(data, '#'))) = [];
        data(data == "") = [];
        data_temp = str2num(char(data(:)));

        %Filter out data coming from substrate

        data_temp(data_temp < 2000) = 0;
        data_temp(data_temp > 80000) = 0;

        data_numeric = [data_numeric; data_temp];

    end
```

```
non_zero_data = data_numeric(data_numeric ~= 0);

mean_d = mean(non_zero_data);
std_d = std(non_zero_data);
figure
boxplot(non_zero_data);
ylabel({'Young s modulus (kPa)'},'fontsize', 10);
set(gca, 'FontSize', 10)
ylim([0 85000])
x0=10;
y0=10;
width = 600;
height = 600;
set (gcf, 'position', [x0,y0,width,height])

%Transform data so its distribution becomes realtively normal
non_zero_data = log10(non_zero_data);

figure
h = histogram(non_zero_data, num_bins, 'Normalization', 'probability');
xlabel({'Young''s modulus (Pa)'},'fontsize', 10);
ylabel({'Count'},'fontsize', 10);
set(gca, 'FontSize', 10)
xlim([3.21 5])
ylim([0 0.025])
x0=10;
y0=10;
width = 600;
height = 600;
set (gcf, 'position', [x0,y0,width,height])
title ({'Condition: '})

figure

histfit(non_zero_data, num_bins);
xlim([3.2 5])

xlabel({'Young''s modulus (Pa)'},'fontsize', 10);
ylabel({'Count'},'fontsize', 10);
set(gca, 'FontSize', 10)
x0=10;
y0=10;
width = 600;
height = 600;
set (gcf, 'position', [x0,y0,width,height])


end
```

## F. FFM probe usage

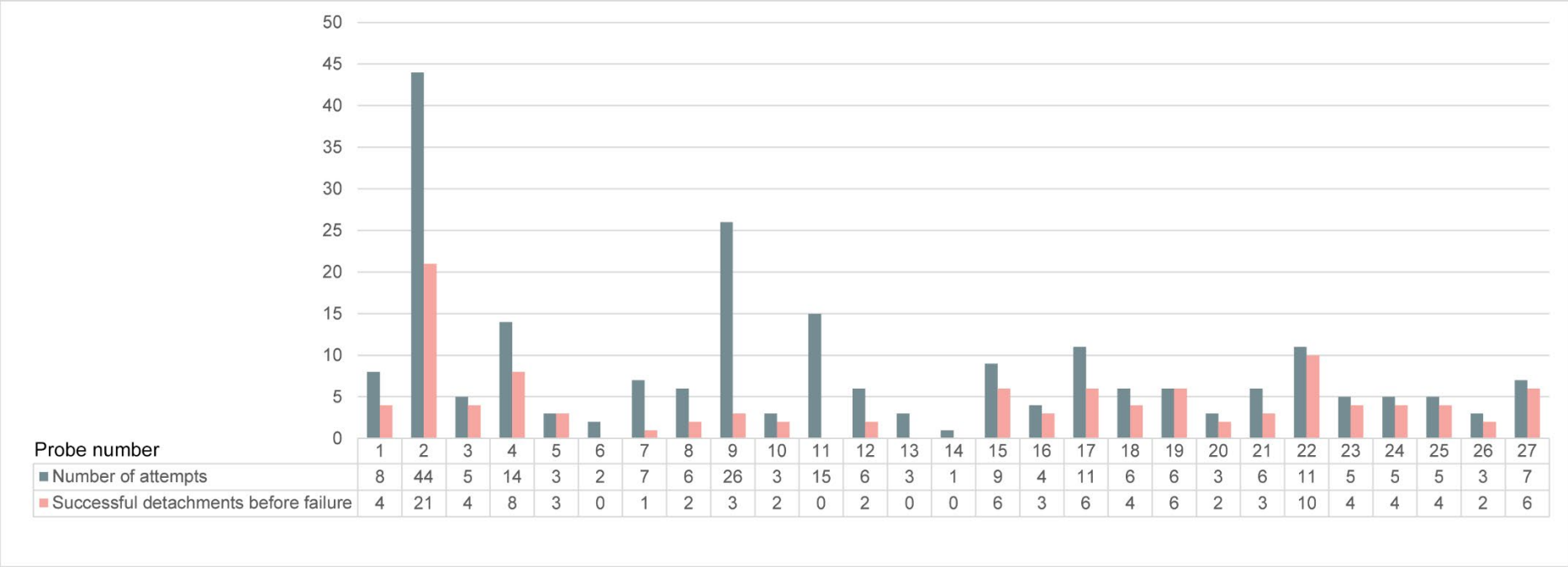


| Probe number | 1 | 2 | 3 | 4 | 5 | 6 | 7 | 8 | 9 | 10 | 11 | 12 | 13 | 14 | 15 | 16 | 17 | 18 | 19 | 20 | 21 | 22 | 23 | 24 | 25 | 26 | 27 |
|---|---|---|---|---|---|---|---|---|---|---|---|---|---|---|---|---|---|---|---|---|---|---|---|---|---|---|---|
| Number of attempts | 8 | 44 | 5 | 14 | 3 | 2 | 7 | 6 | 26 | 3 | 15 | 6 | 3 | 1 | 9 | 4 | 11 | 6 | 6 | 3 | 6 | 11 | 5 | 5 | 5 | 3 | 7 |
| Successful detachments before failure | 4 | 21 | 4 | 8 | 3 | 0 | 1 | 2 | 3 | 2 | 0 | 2 | 0 | 0 | 6 | 3 | 6 | 4 | 6 | 2 | 3 | 10 | 4 | 4 | 4 | 2 | 6 |

**Figure 13** Probe usage summary. On average, one probe was used to detach 4 cells, with a success rate of approximately 54%. The most come mode of failure was micro-channel clogging. Four probes (probe 1, 2, 10 and 14) were damaged during handling of the probe or during the initial approach phase of the experiments.

# G. FFM experimental protocol

### *1. Requirements*

*1.1 Equipment*

- Cytosurge FluiFM Pipette
- AFM + CellHesion module connected
- Petri dish heater
- Vacuum pump
- OB1 pressure controller
- Microfluidic tubing

*1.2 Reagents*

- 1 ml pipette + pipette tips
- 1 x 15 ml tube of 2x filtered DI water
- 3 ml α-MEM

### *2. Procedure*

*2.1 Prepare AFM stage*

- Take a broken Cytosurge FluidFM Pipette probe and load it on the probe holder
- Place probe holder in JPK external support
- Position the probe on the holder by gently pushing down the two side plastic arms
- Make sure the stage is far away from the surface and load the holder with the probe in the JPK system (without any tubes attached)
- Put an empty petri dish in the heating petri dish holder and move the microscope up until it almost touches the back side of the petri dish.
- The center of the petri dish needs to be to the left of the microscope objective
- Place the AFM module in place: 1$^{st}$ rear leg, 2$^{nd}$ left leg, 3$^{rd}$ right leg. Before you lower the third leg make sure no components touch the sides of the petri dish
- Move the probe up or down so the probe edge is in focus (do not move the microscope)
- Remove the JPK stage and the broken probe

*2.2. Load probe*

- Place holder in external JPK support
- Add silicone skirt
- Position the probe on the holder (from the top by gently pressing down on the two plastic arms of the tip)
- With a pipette add 2x filtered DI water to the open channel of the probe
- Remove holder from support and attach tygon tube to the probe
- Approach the plastic end of tube to tip connection point, rotated 90$^{o}$ anticlockwise from horizontal position; align O ring with the aperture in the tip device
- Gently rotate the tube end piece clockwise 90$^{o}$. If the tube side of the connection does not slide in place, take the two components away and try again
- Load the holder in the AFM module

- Connect the free end of the tube to the purple plastic connector and place the plastic connector in its designated place next to the AFM stage leg

*2.3. F-D curve on single cells*

- OPEN PRESSURE CONTROLLER VALVE
- Keep the dry, clean petri dish in the holder
- Place the AFM module in place: 1st rear leg, 2nd left leg, 3rd right leg. Before you lower the third leg make sure no components touch the sides of the petri dish. Focus on the probe tip (there should be small adjustments only since the focal plane is more or less on the probe from the preparation part)
- Apply over pressure (500-800 mbar) and check for water dispense. If the probe is new and water is not coming out, pulsate the pressure a few times
- Align laser with the tip of the probe. Maximize laser signal
- Remove the JPK stage and add the petri dish with the cells. Add 1.5 ml medium and turn on the heater
- Place the JPK stage back. If the laser signal dropped it means the probe is in liquid. Re-align the laser and maximize the sum. Calibrate the probe. If the probe is not in liquid, approach the surface in small increments until the laser sum drops.
- If you have cells on your surface, focus on the cells and manually send the probe towards the surface in 100 um steps. Before it gets into focus, stop and start the automatic approach (set the setpoint to 50 nN)
- If you can not focus on the cells or on anything on the surface, only use the automatic approach (the laser may shift as the probe gets deeper in the liquid. Make sure you re-align it). Once the probe touched the surface, move upwards once.
- In contact mode, start with the following parameters (in advanced settings): setpoint = 50 nN, approach speed = 1 um/s, z length = 80 um, delay time = 10 s, retract speed = 1 um/s, z length = 80 um.
- Prepare the pressure channel: p = -800 mbar (plug the vacuum pump in)
- Use the bottom part of the system to find a cell (keep in mind the probe has a large foot print so it may clash with the walls of the petri dish)
- Once the cell is found, approach once more next to it. After the tip touches the surface, move once upwards again and position the aperture over the nucleus of the cell
- Start the tip approach, once it touches the cell turn the pressure on
- Once the cell has been detached, apply an overpressure of 800 mbar
- Move the stage 3 times up (300 um upwards) and remove the JPK stage. With big round and slow gestures (you actually need to move like this) disconnect the tygon tube and gently pull the probe off the holder.
- Carefully place the probe in Terg-a-zyme (that must be prepared on the day) for 2 minutes in a 24-well plate. After 2 minutes rinse once in 2x filtered DI water and with the same round gentle moves, place the probe back on the holder. The system is ready to be used again.

*2.4. Probe removal*

- Remove JPK module and detach the tube from the connector. Make sure your hand sits on a stable point so that you do not end up pulling too strongly when the tube gets loose
- Gently grab the holder and the probe and rotate it out of place. First disconnect the tygon tube (rotate the plastic part anticlockwise)
- Place the holder in external JPK support and remove the probe. Place the probe in fresh Terg-a-zyme.
- In the meantime, clean the cells and the components that got in contact with the medium

- Remove probe from Terg-a-zyme, rinse it with 2x filtered DI water and place it in 2% PS solution
- If the probe is going to be stored for more than 1 night, place some parafilm over it

## H. FFM FD curve processing MATLAB code

```
close all
clear

%Select the file to plot
%The code will firstly extract the numerical data from the text files

file_name = input('Text file containing the data of interest ', 's');
fid = fopen(file_name, 'r');
if fid == -1
  error('Cannot open file fpr reading: %s', FileName);
end
DataC = textscan(fid, '%s', 'delimiter', '\n', 'whitespace', '');
data  = DataC{1};
fclose(fid);

index_pause = find(contains(data, '# segmentIndex: 1'));
index_retract = find(contains(data, '# segmentIndex: 2'));

data(index_pause:(index_retract-1)) = [];
data(find(contains(data, '#'))) = [];
data(data == "") = [];
data_numeric = str2num(char(data(:)));

VerticalTipPosition = data_numeric(:,1)*(10^6);
VerticalDeflection = data_numeric(:,2)*(10^9);

% Approach end value is depended on the sample rate of the FFM measurement

approach_end = 48000; %this value may need to be adjusted as some approach curves are
not complete.

h = figure('Renderer', 'painters', 'Position', [10 10 900 900]);
plot(VerticalTipPosition(1:approach_end),VerticalDeflection(1:approach_end),'k','LineWi
dth',2)
grid on
xlabel('Vertical tip position (um)','fontsize', 24)
ylabel('Vertical deflection retract (nN)','fontsize', 24)
set(gca,'FontSize',20)
xlim([-15 90])
ylim([-250 150])
hold on
plot(VerticalTipPosition(approach_end+1:end),VerticalDeflection(approach_end+1:end),'b'
,'LineWidth',2)
title({['Cell # (DATE)']})
saveas(h,sprintf('cell#.png'));
```

# I. Submicron patterns SEM images

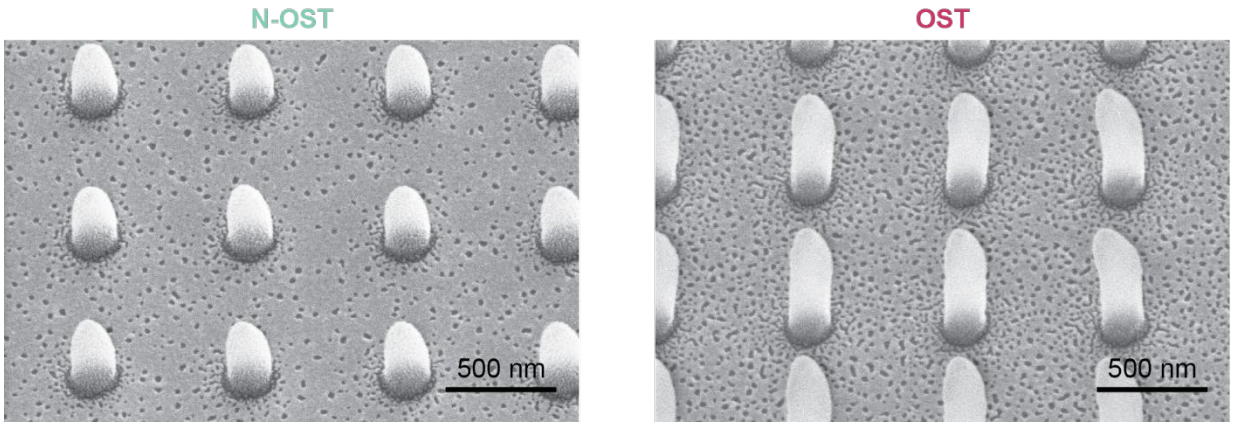


**Figure 14** SEM images of (a) N-OST submicron pattern and (b) OST submicron pattern. The images were acquired at an inclination of 30º. Pillars presented a dome like shape at the tip. This aspect is an artefact of the manufacturing procedure: the laser voxel (volume in which the laser is in focus and the polymerization of the material occurs) is ellipsoidal in shape. If the main body of the pillars are scanned multiple times as the voxel moves upwards, the top of the pillars experience less exposure and thus the polymerized shape follows the shape of the voxel [33].

## J. Adhesion data vs cell idle time

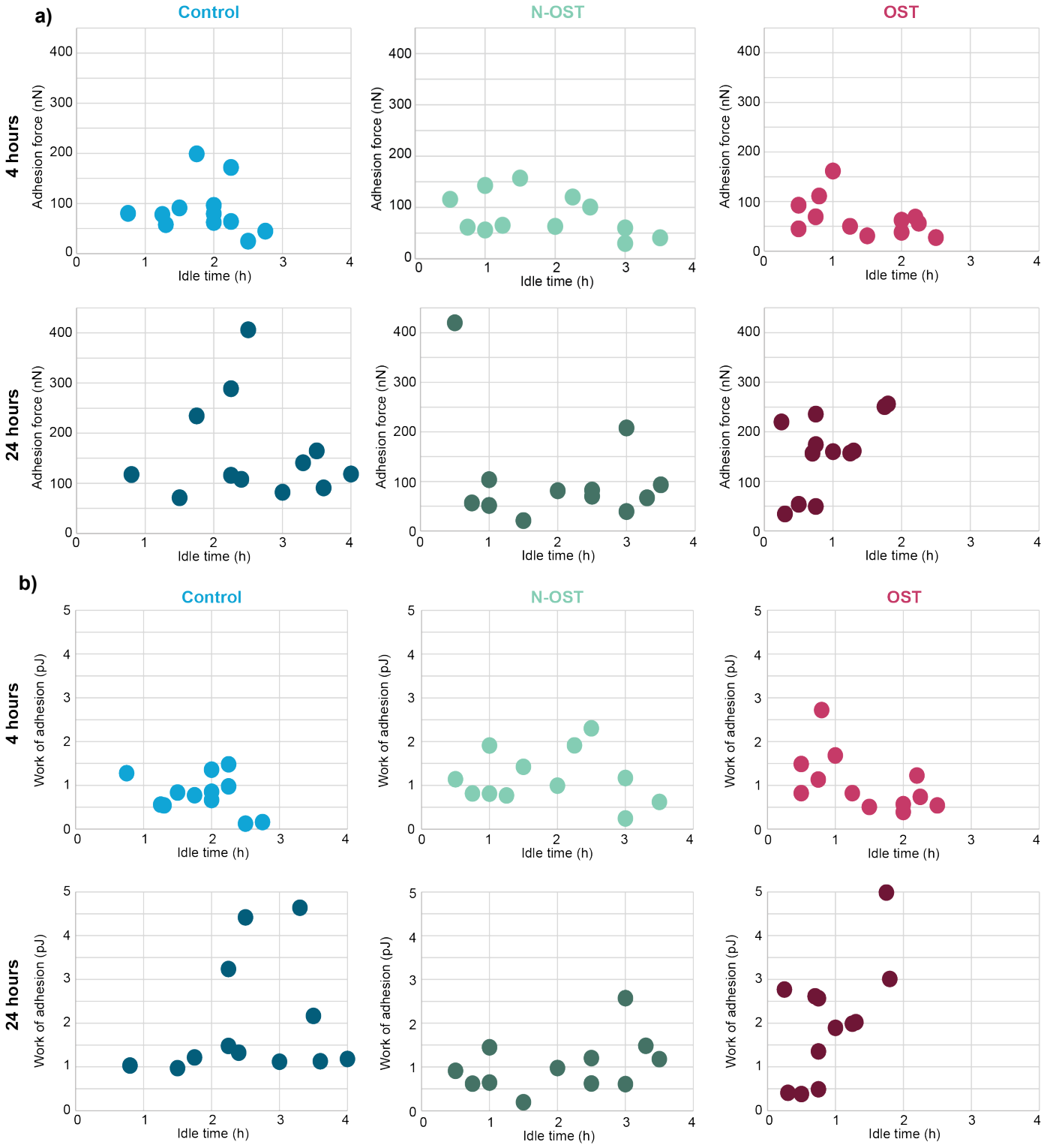


**Figure 15** (a) Adhesion force (nN) (b) Work of adhesion (pJ) plotted against the idle time of measurement, *i.e.,* the time between the moment the cells were taken out of the incubator and the moment a certain detachment measurement was taken. Most of the data points were acquired in an idle time less than or equal to 2 hours. Nevertheless, no trend in the data points can be observed, indicating that adhesion properties have not significantly changed during the experimental day.

## K. Young's modulus per condition - histogram representation

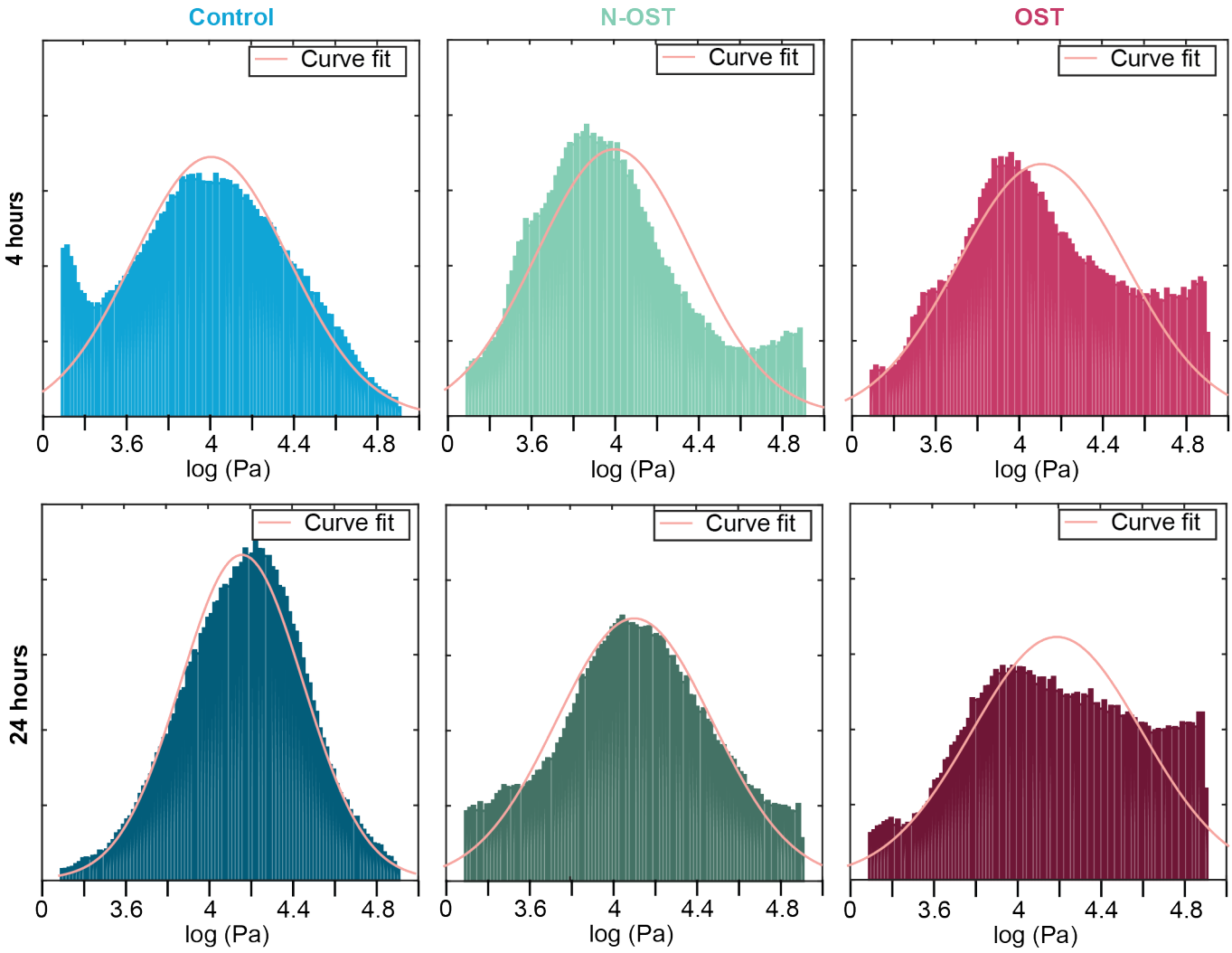


**Figure 16** Histograms representing all the Young's modulus data points recorded per condition (12 cells/condition). Data was transformed with a log10 in order to have a normal representation of data and the histograms were normalized (number of elements in a bin divided by the number of elements in the input data). The histograms captures different contributors to the stiffness (such as fibres as opposed to the nuclear structures) [34]. Nevertheless, the noise induced by the N-OST and OST substrates decreased the reliability of this data representation (Young's modulus data points are present mainly on the right hand side of the maximum peak – this aspect is more evident with the OST data). A better image processing software, that could isolate the cell from the surface in a more effective way, could help increase the reliability of these histograms.